LA 11233-T
Thesis

UC-34C
Issued: March 1988

Theoretical and Experimental Cross Sections for Neutron Reactions on ^{64}Zinc

Debra Ann Rutherford

MASTER

LA--11233-T

DE88 005896

DISCLAIMER

Los Alamos National Laboratory
Los Alamos, New Mexico 87545

ACKNOWLEDGEMENTS

I would like to take this opportunity to thank all the people who encouraged me and supported my efforts throughout this endeavor. A thank you to the late Professor J. Craig Robertson who gave me the opportunity to perform this work, but did not have a chance to see its fruitful outcome. Thank you for your faith in my devotion to scholarship.

I could not have completed this work without the guidance of Dr. Phillip Young, he was a source of inspiration at all times.

Thank you Kathy Brogan for your kindness, friendship and technical expertise.

TABLE OF CONTENTS

Page

LIST OF FIGURES viii

LIST OF TABLES x

1. INTRODUCTION 1

2. NEUTRON SOURCE AND MONITORING 5

2.1 Introduction 5

2.2 General Description of the Texas Nuclear Neutron Generator 6

2.2.1 Ion Source and Gap Lens 6

2.2.2 Accelerating Tube 9

2.2.3 Drift Tube and Target 11

2.3 Neutron Source 11

2.3.1 The (D,T) Reaction 11

2.3.2 Monitoring the Neutron Flux 13

2.4 Radiation Detection System 15

2.4.1 Introduction 15

2.4.2 Description 15

2.4.3 Initial Detector Preparation 18

2.4.4 Correction Factors 19

3. EXPERIMENTAL PROCEDURE AND ANALYTICAL METHODS 26

3.1 Introduction 26

3.2 Calculations 27

3.2.1 Saturated Activity Determination 31

3.2.2 Cross Section Determination 33

3.2.3 Decay Scheme Determination 34

4. THEORETICAL CROSS SECTION ANALYSIS 40

4.1 Introduction 40

4.2 GNASH 40

4.3 Hauser-Feshbach Statistical Model 45

4.4 Level Density Model 51

4.5 Non-equilibrium Reactions 60

4.5.1 Preequilibrium Model 62

4.5.2 Direct Reaction Cross Section Model 62

4.6 The Optical Model and Parameter Determination for the Neutron Optical Model 63

4.7 The Optical Model and Parameter Determination for the Proton and Alpha Optical Model 74

4.8 Gamma Ray Transmission Coefficients 78

5. RESULTS AND CONCLUSIONS 79

5.1 Introduction 79

5.2 Analysis of Experimental Results 79

5.3 Analysis of Theoretical Results 85

5.4 Comparison of Experimental and Theoretical Results 85 86

5.5 Conclusions 92

6. RECOMMENDATIONS FOR FUTURE WORK..... 96

REFERENCES..... 97

LIST OF FIGURES

Page

2.1 Schematic Diagram of the Neutron Generator..... 7

2.2 Diagram of the Gap Lens and Focusing Mechanism..... 10

2.3 Typical Output of Neutron Detector..... 14

2.4 Schematic of the NaI(Tl) Spectrometer..... 16

2.5 Count versus Voltage for the NaI(Tl) Spectrometer..... 20

2.6 Gamma Energy versus Channel Number..... 21

2.7 Long Term Stability of the NaI(Tl) Spectrometer..... 22

3.1 Decay Curve of ^{64}Cu..... 28

3.2 Decay Scheme of ^{63}Zn..... 36

3.3 Decay Scheme of ^{64}Cu..... 37

3.4 Decay Scheme of ^{62}Cu..... 38

4.1 Complex Decay Scheme of ^{65}Zn..... 42

4.2 Level Density Diagram 44

4.3 Schematic Illustration of GNASH Calculational Scheme..... 46

4.4 Schematic Illustration of Compound Nucleus Formation and Decay..... 48

4.5 ^{65}Zn Levels..... 52

4.6 ^{64}Zn Levels..... 53

4.7 ^{63}Zn Levels..... 54

4.8 ^{64}Cu Levels..... 55

4.9 ^{63}Cu Levels..... 56

4.10 ^{61}Ni Levels..... 57

4.11 ^{60}Ni Levels..... 58

4.12 Competing Processes in Compound Nucleus Formation..... 61

4.13 Neutron + Zn Total Cross Sections..... 69

4.14 Neutron + ^{64}Zn Elastic Cross Sections (E_n = 3.44 MeV)..... 70
4.15 Neutron + ^{64}Zn Elastic Cross Sections (E_n = 8.05 MeV)..... 71
4.16 Neutron + ^{64}Zn Elastic Cross Sections (E_n = 14.0 MeV)..... 72
4.17 ^{63}Cu (p,n)^{63}Zn Cross Sections..... 75
4.18 ^{65}Cu (p,n)^{65}Zn Cross Sections..... 76
5.1 ^{64}Zn (n,2n)^{63}Zn Cross Sections..... 87
5.2 ^{64}Zn (n,2n)^{63}Zn Cross Sections..... 88
5.3 ^{64}Zn (n,p)^{64}Cu Cross Sections..... 89
5.4 ^{64}Zn (n,p)^{64}Cu Cross Sections..... 90
5.5 ^{64}Zn (n,p)^{64}Cu Cross Sections..... 91

LIST OF TABLES

Page

3.1 Q Values for Three Reactions..... 30

4.1 Final Neutron Optical Model Parameters..... 73

4.2 Average Resonance Parameters..... 73

4.3 Final Proton Optical Model Parameters..... 77

4.4 Final Alpha Optical Model Parameters..... 77

5.1 Previous ^{64}Zn (n,p)^{64}Cu Cross Section Measurements..... 81

5.2 Previous ^{64}Zn (n,2n)^{63}Zn Cross Section Measurements..... 83

5.3 Error Contributions in the Cross Section Measurements..... 84

5.4 Individual Data Sets used to Analyze the ^{64}Zn (n,2n)^{63}Zn Cross Section Measurements..... 94

5.5 Individual Data Sets used to Analyze the ^{64}Zn (n,p)^{64}Cu Cross Section Measurements..... 95

THEORETICAL AND EXPERIMENTAL CROSS SECTIONS FOR NEUTRON REACTIONS ON ^{64}ZINC

DEBRA ANN RUTHERFORD

Abstract

Accurate measurements of the $^{64}Zn\ (n,2n)^{63}Zn$ and $^{64}Zn\ (n,p)^{64}Cu$ cross sections at 14.8 MeV have been made using a Texas Nuclear Neutron Generator and the activation technique. A NaI(Tl) spectrometer (using two 6" x 6" NaI detectors/crystals) was used to measure the gammma radiation emitted in coincidence from the positron-emitting decay products. The measurements were made relative to $^{65}Cu\ (n,2n)^{64}Cu$ and $^{63}Cu\ (n,2n)^{62}Cu$ cross sections, which have simlar half-lives, radiation emission, and were previously measured to high accuracy (2 percent). The value obtained for the (n,2n) measurement was 199 $\pm$ 6 millibarns, and a value of 176 $\pm$ 4.5 millibarns was obtained for the (n,p) measurement. In concert, a theoretical analysis of neutron induced reactions on ^{64}Zn was performed at Los Alamos National Laboratory using the Hauser-Feshbach statistical theory in the GNASH code over an energy range of 100 keV to 20 MeV. Calculations included width fluctuation corrections, direct reaction contributions, and preequilibrium corrections above 6 MeV. Neutron optical model potentials were determined for zinc. The theoretical values agree with the new 14.8 MeV measurements approximately within experimental error, with calculations of 201 millibarns for the (n,2n) cross section and 170 millibarns for the (n,p) cross section Results from the analysis will be made available in National Evaluated Nuclear Data Format (ENDF/B) for fusion energy applications.

CHAPTER ONE

INTRODUCTION

Cross section data is fundamental for many types of research, ranging from nuclear weapons testing to fusion research; consequently in order to fulfill the needs for nuclear data, cross section analyses have been prioritized by the Nuclear Data Committee [1]. In addition to this committee's work, in 1982 the Department of Energy initiated a program entitled, "Coordination of Magnetic Fusion Energy Nuclear Data Needs and Activities," that not only determined the nuclear data needs but also prioritized these needs for magnetic fusion [2]. The requested measurements should be the most applicable to the fusion blanket and the shield development. One of these highly prioritized interactions is the ^{64}Zn (n,p) ^{64}Cu cross section which provides dosimetry and activation data for the fission and fusion community. This cross section and the ^{64}Zn (n,2n) ^{63}Zn cross section were measured for this work.

A neutron cross section is defined as a measured or calculated probability that a neutron will interact with a nucleus; thus, a cross section can also be referred to as the effective interaction area. This latter definition of a cross section coincides with the Democritan-Lucretian view of "atomism" which states that there are certain ultimate particles [$\alpha\tau\mu$os] that are indivisible and interact with everything to make life as it is known. In fact, Lucretius said in ~ 50 B.C.: "But as it is, because the bonds between the atoms differ and matter itself is eternal, a thing remains with its body uninjured until assailed by a force whose keeness is a match for its own structure. Therefore no thing is reduced to nothing, but all things change back into particles

of matter [3]." This research then, was generally undertaken in the spirit of philosophical deduction and experimental research to provide measurements of cross sections as fundamentals for the scientific world. Specific steps, included remeasuring the ^{64}Zn (n,2n) ^{63}Zn interaction as a standard for the University of New Mexico activation analysis system and the ^{64}Zn (n,p) ^{64}Cu cross section for use in the fusion reactor program [4]. Although experimental data already exist for these two isotopes at 14.8 MeV, these data have large error bars; consequently the present work is an attempt to produce a more precise data base [5]. After these measurements were performed, the data derived from them were compared to theoretical calculations performed by the GNASH code [6].

A primary purpose of this research is to develop a method for experimentally determining the cross sections through activation analysis. This process can best be described as the bombardment of the test element by neutrons within the 14.84 MeV +/- 20 keV range to produce radioactive isotopes [4]. Each isotope produced through the interaction of the element and the neutrons has a characteristic half-life and emission spectrum. The half-life and the radiation emitted, then, enables the researcher to determine the interaction (cross section) that took place, through calculations. Thus, one measures the probability of high energy neutrons interacting with an element to form the radioactive isotopes. This cross section can also be called the "activation cross section." Since the neutron's wavelength at this energy is less than the size of the nucleus and approximately the size of the neutron itself, the cross section is approximately equal to the geometrical size of the nucleus.

Other intrinsic elements playing major roles in this research, are the activation cross sections for two copper isotopes previously measured by Ghanbari and Robertson who used the exact same experimental setup [7]. Their measurements not only serve as a standard but also determine the neutron energy and flux. These reference foils analysed by Ghanbari and Robertson were separated isotopes of ^{63}Cu and ^{65}Cu. The reactions that were previously analyzed were: ^{63}Cu (n,2n) ^{62}Cu, and ^{65}Cu (n,2n) ^{64}Cu. The foils were isotopically (99.99 percent) pure.

Once activated, these foils were analyzed using the gamma-gamma coincidence method which actually measures the beta-plus activity associated with the decay scheme of the product nuclide. This system was established by Ghanbari and Robertson for this purpose [4]. Initially, their cross sections were measured using the 4-pi beta gamma counter and the gamma-gamma counter. For the purpose of the present experiment, however, only the gamma-gamma coincidence system was used because of the systematic error intrinsic to the 4-pi beta-gamma coincidence system [7].

After the experimental section of the work was completed, the measured cross section values were compared with the theoretical values obtained using the GNASH code developed by Young and Arthur [6] . This code, described in Chapter Four, calculates many different cross sections by theoretically "modeling" these interactions between particles and isotopes. This technique was applied to the previously delineated (n,2n) and (n,p) cross sections with energies from 100 keV to 20 MeV. In this project the GNASH code provided the following calculations: ^{64}Zn (n,2n) ^{63}Zn, ^{64}Zn (n,p) ^{64}Cu, ^{64}Zn (n,nα) ^{61}Ni, ^{64}Zn (n,np) ^{63}Cu, ^{64}Zn (n,γ) ^{64}Zn, etc.

An advantage of the GNASH code is that it allows competing reactions to be simultaneously calculated; therefore other cross sections that are impossible to determine experimentally are calculated here. The code permits dynamic modeling of the competing processes, with spin, parity, level densities, all being simultaneously considered. Another advantage of the GNASH code is that it has already been used to analyze several other cross sections for elements and isotopes [8]. This previously established data shows that theoretical calculations are important for areas where no experimental data exists or where there is reasonable uncertainty in the data itself. A brief description of the code enables the reader to become familiar with the details of the codes capabilities and limitations, while actually working on the problem of analyzing the reactions previously discussed. The experimental and theoretical values provided by this research will provide other researchers with a more accurate data base for the zinc istotopes.

The remainder of this thesis is divided into four chapters. Chapter Two gives a detailed description of the neutron source and gamma spectrometer used in the experimental section of this work. Chapter Three explains the details of various physics for the cross section determinations as well as discussing the method for experimentally calculating cross sections through activation analysis. Chapter Four discusses the GNASH code and describes the calculations used to theoretically model interactions between particles. Chapter Five concludes the thesis by discussing the results of the theoretical and experimental sections and also a comparison of these results. Finally, there is a section suggesting recommendations for future research.

CHAPTER TWO

NEUTRON SOURCE AND MONITORING

2.1 Introduction

In order to understand the experimental set-up, one must first understand the purpose that it serves. The purpose is to use an experimental technique called "activation analysis" to measure cross sections. As the name implies, the experimenter took a sample that was stable and irradiated it with neutrons until it became sufficiently radioactive. The radioactive emission from the sample was then analyzed by a radiation detector capable of determining the intensity and the energy of the radiation emitted. Known principles along with the measured parameters allow the experimenter to calculate fundamentals, which determine the activation cross section. In this case, stable zinc foils were irradiated to form isotopes of zinc and copper. The beta-plus radiation emitted from these foils was measured along with the radiation from a similar standard (^{63}Cu or ^{65}Cu) with a known cross section which was irradiated at the same time. Since the known standard was very similar, it was used as a reference to calculate the cross section for the isotopes produced [7].

A more accurate reaction cross section was determined for production of zinc and copper by applying correction factors. The measurements conducted in this research used standard equipment including a Texas Nuclear Neutron Generator and gamma ray spectrometer available at the University of New Mexico Nuclear Engineering Laboratory. Activation analysis, therefore, required a neutron source, a well measured standard, and a radiation detection system.

2.2 General Description of the Texas Nuclear Neutron Generator

The Texas Nuclear Neutron Generator (TNNG) was used as the source of neutrons. It produced a high flux of neutrons through the continuous bombardment of a tritiated-titanium target with deuterons. The 14.8 MeV neutrons were produced by the well known D-T reaction [9]:

$$^{2}_{D} + ^{3}_{H} = ^{4}_{He} + ^{1}_{0}n \qquad (2.1)$$

In order to better understand the neutron generator, each of the main components will be described in detail along with its function. The main components of the generator itself were an ion source, an accelerating tube, and the target. The supporting mechanisms of the generator were the high voltage supply, the vacuum system, and the remote control console. Since the generator provided a high flux of high energy neutrons, it was also important to have adequate radiation shielding.

The neutron generator was set up in the Nuclear Engineering Laboratory Hot Cell. The controls for the generator were located outside of the cell which also included the control and diagnotic devices for the plastic scintillator that was used to monitor the neutron flux.

2.2.1 Ion Source and Gap Lens

The ion source consisted of a series of components as shown in Figure 2.1. The deuterium gas (99.9 percent pure), palladium leak,

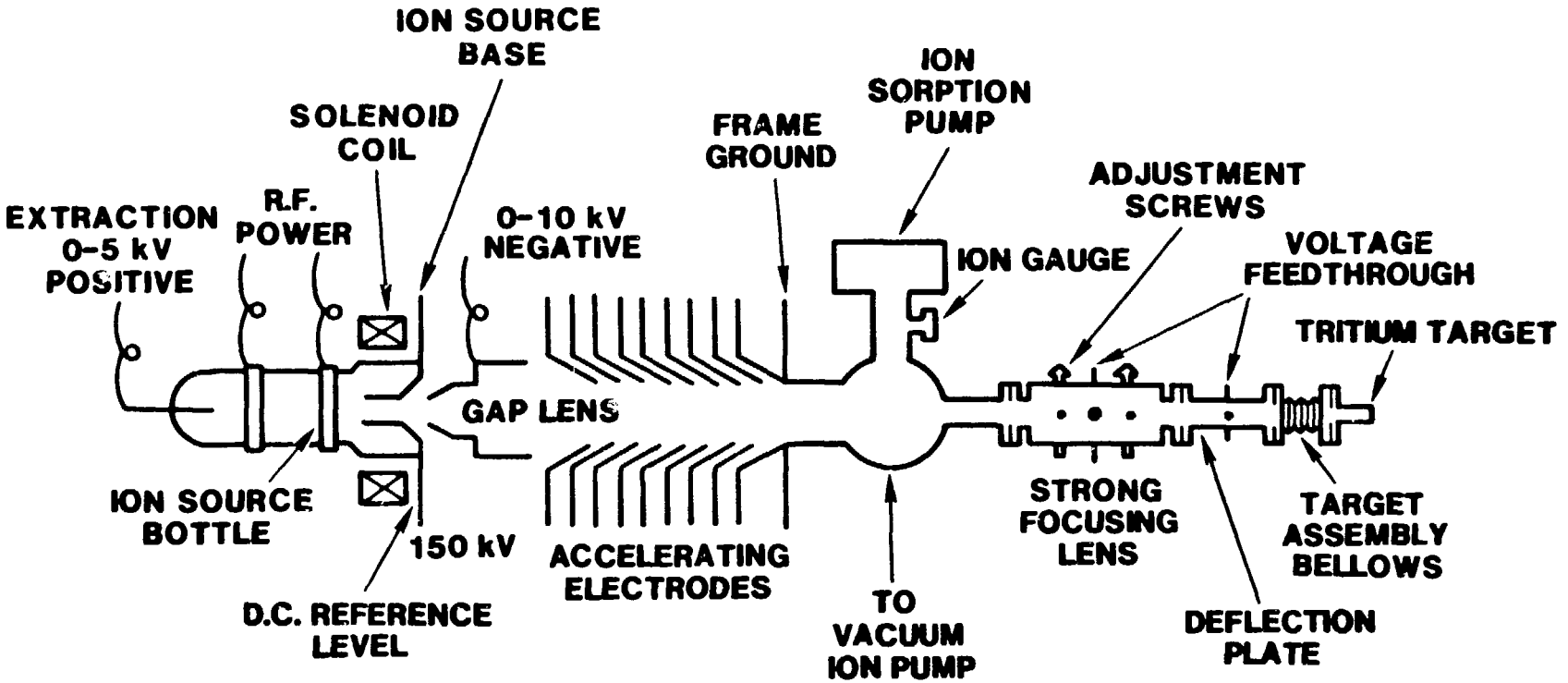

Figure 2.1 Major Components of the Texas Nuclear Neutron Generator

pyrex bottle, r-f oscillator, solenoid, and the quartz sleeve were the major components.

These components were operated in the following way: deuterium gas was introduced into the system by activating the paladium leak. The palladium allowed rapid diffusion of the deuterium molecules when it was heated. The temperature was controlled by the heating coil surrounding the palladium leak. As the temperature was increased, more deuterium was admitted into the pyrex tube. Since the tube and the gas supply were at different pressures, the gas naturally flowed into the tube which was at a much lower pressure.

Once the deuterium was introduced into the pyrex tube, the radio frequency field was used to ionize the deuterium gas. This ionization was accomplished by activating the two excitor rings which fit around the bottle, as shown in Figure 2.1. Electromagnetic energy was coupled through the pyrex glass tube, thus exciting the deuterium gas. The deterium gas was excited to the point where it disassociated and became ionized emitting the characteristic deep reddish/purple light of the deuterium spectra.

Next, these ions were forced into the exit canal by the positive potential across the bottle. A solenoid which fit around the bottle, produced an axial magnetic field; this, in turn produced a force in the radial direction of the bottle due to the Lorentz force ($F = v \times B$). This restricted the ions path to the center of the bottle.

The quartz sleeve at the end of the aluminum exit canal prevented the recombination of the ions. It also acted as a focusing agent for the ions. The electric force, then, focused and directed the ions so that they did not hit the canal walls.

The ion beam expanded due to space charge (repulsive) forces at the exit of the canal since focusing was no longer applied. Therefore, another focusing agent was needed to aid the ions on their path to the accelerating tube. This apparatus was the gap lens. By applying voltage to the gap lens, the beam was focused into the accelerating tube. This is shown schematically in Figure 2.2.

2.2.2 **Accelerating Tube**

Once the beam was produced and focused it then entered the accelerating tube, as shown in Figure 2.1, designed for multi-stage acceleration of the positive ions. As stated previously, the ions must have enough energy to achieve the (d,t) reaction; consequently, they must be accelerated to 150 kV. The accelerating tube on the neutron generator was designed for up to 150 kV operation. The tube was divided into 20 electrodes which were separated by porcelain insulators. This division of the voltage insured that each time the ions passed the electrode, they received a 7.5 kV increase in energy. Identical resistors were placed between each electrode to insure equal voltage division among the electrodes. The resistors were mounted in a lucite stack holder alongside the tube. The total current drawn by the resistor stack at 150 kV was 750 micro-amps. There were twenty 10 mega-ohm resistors in the stack. The tube also focused the ions as they were accelerated.

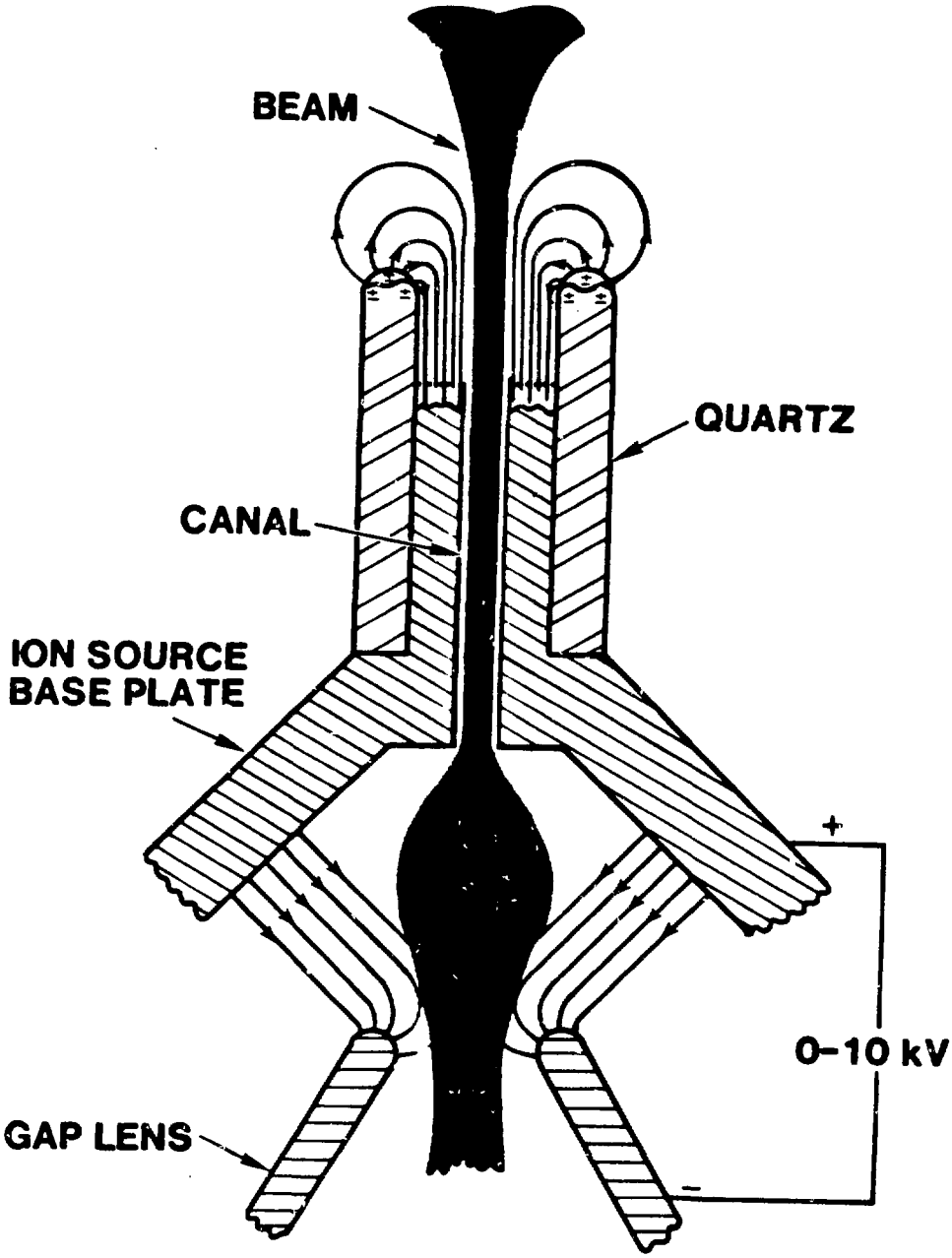

Figure 2.2 Schematic of Gap Lens

2.2.3 **Drift Tube and Target**

The Texas Nuclear Neutron Generator also had a drift tube section located just after the ions came out of the accelerating tube. This section held at vacuum (4×10^{-7} torr), so that foreign molecules did not contaminate the ion beam. An ion pump provided a high vacuum. Bellows in the middle of the drift tube allowed the experimenter to adjust the tube for maximum beam transmission to the target. Finally, the tritiated/titanium target was located at the end of the drift tube.

The target was a 1-1/4" diameter disk. The tritium gas was occluded in a very thin layer of titanium, which had been evaporated onto copper. In this research the tritium activity upon insertion into the TNNG was 5 Curies.

2.3. **Neutron Source**

2.3.1 **The (D,T) Reaction**

It is well documented that the Q value of the D-T reaction is +17.6 MeV [10]. Since the deuteron energy at the interaction point is small compared with the Q value of the reaction, the neutrons produced are essentially monoenergetic. The product energy varies inversely with the product mass; consequently, the neutron carries off the majority of the reaction energy. For th's experiment, the Texas Nuclear Neutron Generator, produced neutrons at approximately 14.8 MeV [4].

The D-T reaction is an excellent source of high energy neutrons. It was chosen over a D-D source for several reasons. First, the yield from the D-T reaction is much greater than that of the D-D reaction. The D-D cross section at 150 keV is 3.0×10^{-26} cm^2/atom, as compared to the D-T cross section of 4.55×10^{-24} cm^2/ atom [11]. The neutron output for a thin D-T target compared to a D-D target is approximately 300 times greater. Since activation analysis depends upon a prolific neutron flux, the D-T reaction is the one chosen for the generator at 14.8 MeV. The D-D reaction is better for lower energy reactions.

The target must be thin enough so that it will not interfere with the outgoing neutrons, yet it must be thick enough to actually stop the incoming deuterons. If the target thickness is increased too much, the flux actually decreases.

Also, as noted by Ghanbari, the neutron energy is a weak function of laboratory angle [4]. However, this observation was not important for this research because all of the experiments were done at 0 degrees.

Once the neutron flux has been satisfactorily established, the distribution that the samples see must be examined, so that a minimum of interference can be established between the neutron flux and the foils. Since the tritium target must be cooled, the TNNG has an outlet and a water jacket for target cooling. Because the water would thermalize the neutrons, high pressure air emitted from a copper nozzle was chosen to cool the target. This would provide a minimum amount of interference in the neutron flux. Ghanbari and Robertson also showed that the neutron flux followed a $1/r^2$ behavior [4]. This was done by irradiating Fe foils and measuring that cross section as a function of distance (r).

It is also important to note that the target lasts approximately 10 hours of operation before it depletes substantially.

2.3.2 **Monitoring the Neutron Flux**

The flux monitor used in this experiment was a plastic scintillator. This is a fast neutron detector mounted on the wall of the hot cell approximately 2 meters from the target. The plastic slows down the neutrons so that they can be detected by the LiI(Eu) scintillation detector. The scintillator light is converted into an electrical signal that can be amplified by a photomultiplier tube. A typical output recorded by the plastic scintillator can be seen in Figure 2.3.

A fast neutron detector works on the principle that it first slows down the neutron with sufficient moderating material so that it can detect the neutrons with reasonable efficiency. The incoming 14.8 MeV neutrons lose most of their energy in the moderator before they are counted. However, the moderator must not be too thick; otherwise the neutron will be slowed to a point that it will not even reach the detector. This large plastic scintillator fulfills each of the above requirements.

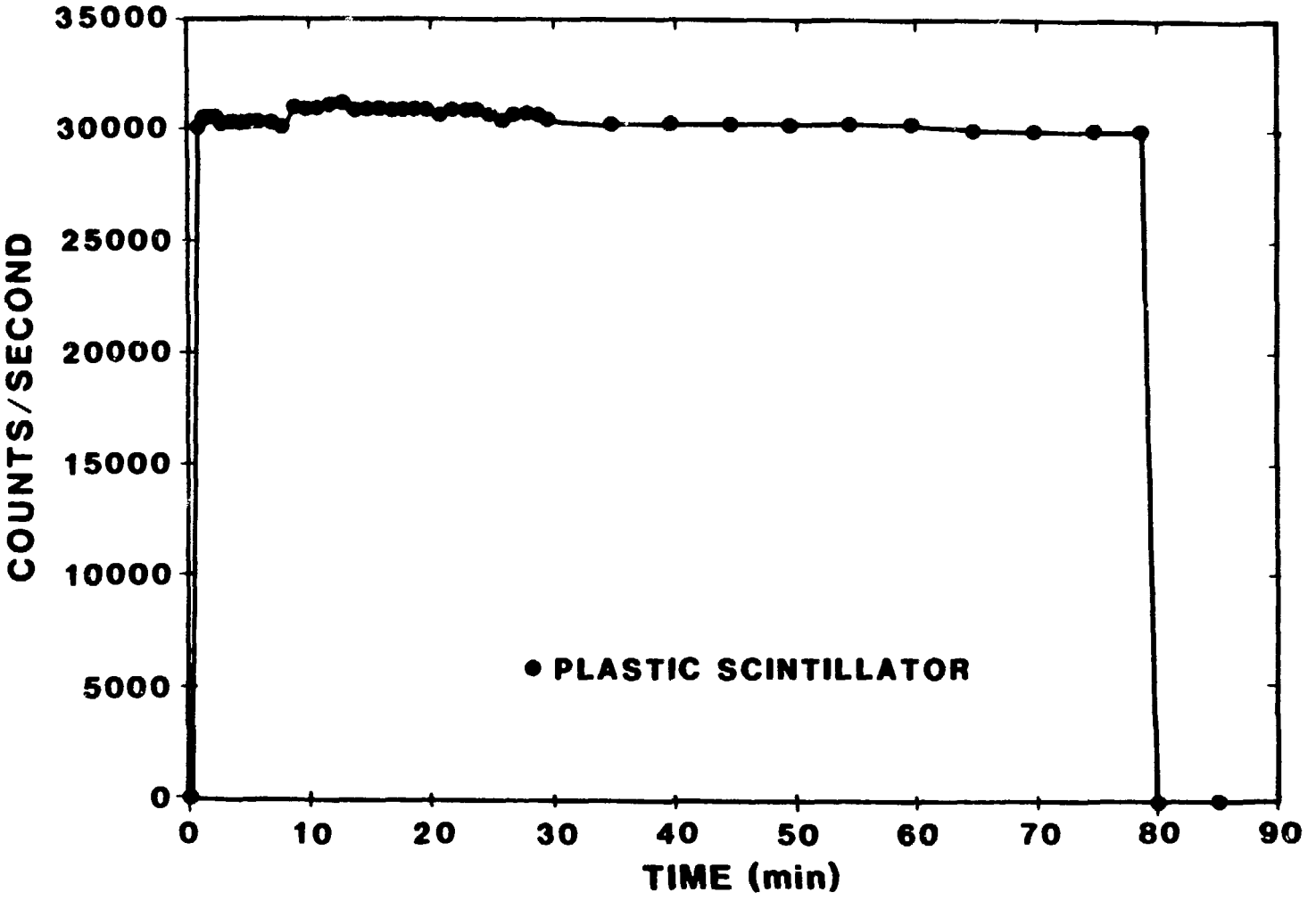

Figure 2.3 Neutron Output as Recorded by the Neutron Monitor (Plastic Scintillator)

2.4 Radiation Detection System

The NaI(Tl) Spectrometer

2.4.1 Introduction

The radiation detection system that was used to determine the activity from the irradiated samples was a gamma-gamma coincidence system [4]. The system consists of two 6 inch diameter by 6 inch long NaI scintillation detectors, placed exactly 180 degrees from each other and accompanied by electronic diagnostics. The scintillation crystals are surrounded by lead shield to keep the gamma ray background radiation as low as possible. The NaI(Tl) Spectrometer or gamma-gamma coincidence unit as seen in Figure 2.4 is located in a room next to the Hot Cell to insure low gamma ray background.

2.4.2 Description

Each of the crystals is hooked up to a preamplifier, amplifier, single-channel analyzer, and finally in concert to a coincidence unit. Figure 2.4 shows a schematic of the gamma-gamma coincidence system. Power is provided to the two photomultiplier tubes by a Fluke 415B high voltage power supply.

The detection system chosen for this work had to be one that measured the characteristic radiation emitted from the sample; in this case gamma rays were produced through annihilation radiation of positrons emitted from the radioactive product nuclei in the experiment.

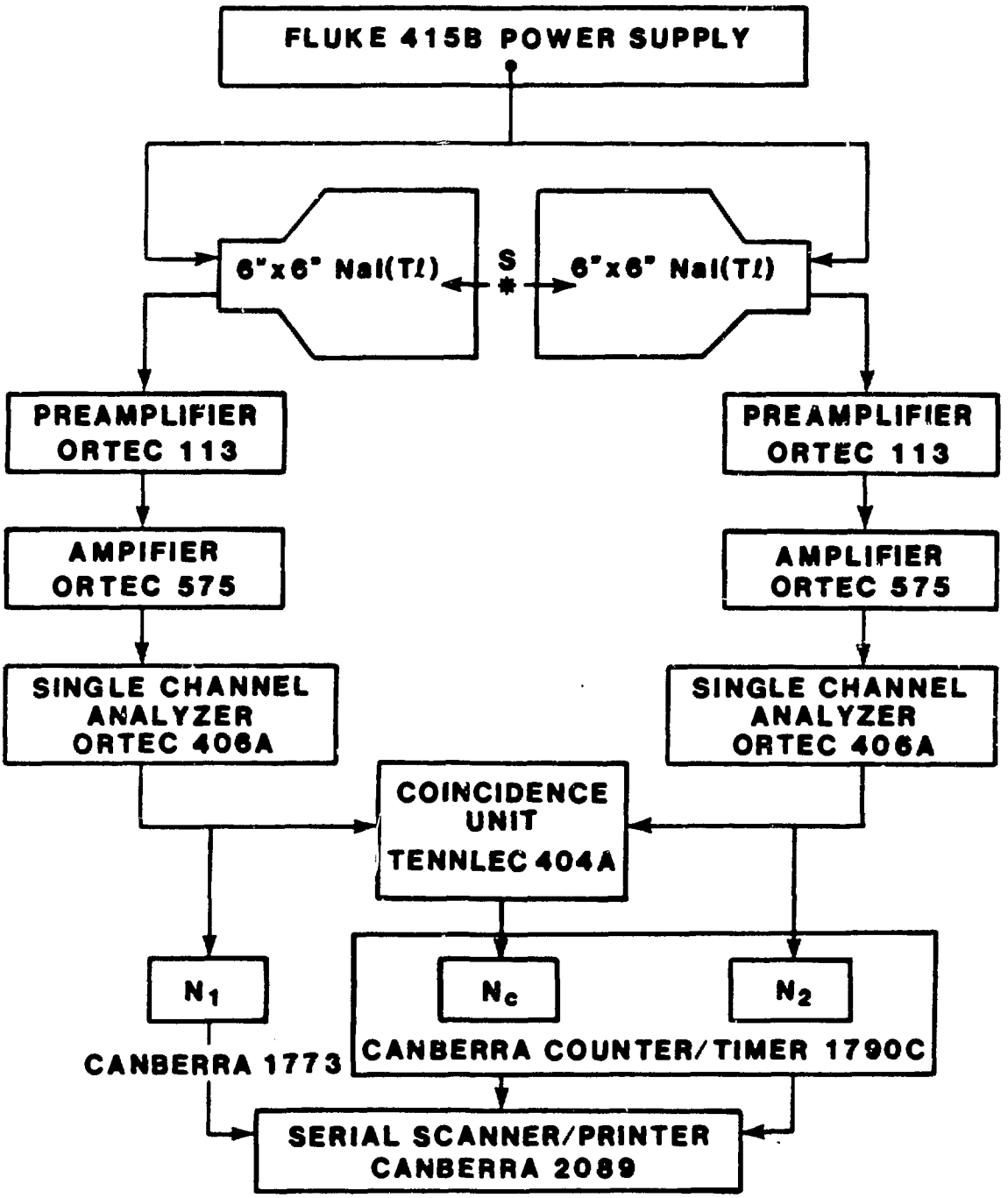

Figure 2.4 Schematic Diagram of the NaI (Tl) Spectrometer

A positron is defined as a particle with the same mass as an electron and with an electric charge equal in magnitude but opposite in sign to that of the familiar electron. It is produced by the following means: a photon of sufficient energy can raise an electron from a state of negative energy to that of positive energy. When the electron disappears from its negative energy state, it leaves a "hole", which means that a positron appears. Therefore, a pair of particles are created: the electron-positron pair. The reverse process is defined as annihilation radiation. Once the positron is formed, it interacts with other particles until it is almost at rest. It then interacts with an electron in the same energy state. They "annihilate" each other and simultaneously two gamma-rays with 0.511 MeV energy are emitted in opposite directions. These two gamma rays energies are equal to the rest mass of an electron.

A gamma ray is uncharged and does not to any extent ionize the material that it passes through. Therefore, it is imperative that a detector for the gamma rays enables it to transfer all of its energy to an electron in an absorbing material. Since a scintillation detector must be able to convert the radiation detected into light, a crystal detector was chosen that has several outstanding capabilities. NaI (Tl) was chosen because of its excellent light yield and because it has an excellent response in the energy range of interest, in this case 0.511 MeV [10]. The conversion of radiation into light pulses should also be linear with increasing energy. The 6 inch by 6 inch crystal also had to be big enough to catch all or most of the radiation emitted from the sample. Of course, the detectors must be stable over a long period of time; this has been established from prior experiments. This detector

fulfills all of the above requirements for measuring the radiation emitted from samples.

Although other detectors fulfill some requirements, they did not fulfill all the requirements for the research. For example, if only one Ge(Li) detector were available, coincidence capability would be sacraficed, and this is the essential part of the detection system. Thus, there had to be two detectors large enough to catch all of the emmitted radiation surrounding the sample. Even though the Ge(Li) detector is more sensitive to gamma rays at lower energies, it was not practical for this measurement. Therefore, the germanium lithium detector which is generally used for analyzing more complex spectra was used in the present experiment.

2.4.3 **Initial Detector Preparation**

As with any detector certain procedures must be followed to insure that it is set up properly. For this system, the steps were as follows: 1) measuring the voltage plateau, 2) determining the linearity, 3) determining the resolution, 4) determining the detection efficiency, and finally 5) determining the long term stability of the system.

The operating voltage of the detectors was found by measuring the voltage plateau. Since Na-22 emits the same radiation as the irradiated samples, a Na-22 source was used to perform this experiment. The source was placed between the detectors and the count rate was noted as the experimenter slowly increased the photomultiplier tube bias voltage. As

in any detector system there is a point where the count no longer increases; this is called the "counting plateau", which determines the operating voltage for the system. In this case, it was 995 volts. See Figure 2.5. These steps were followed for both detectors.

Next, the linearity of the system was determined by placing various gamma emitters between the detectors and recording their channel number on the multi-channel analyzer. The isotopes which were used are available in most laboratories; Na-22, Co-59, Co-60, Cs-137, etc. See Figure 2.6. This was also checked with an oscilliscope to see that the pulse height was linear as a function the gamma ray energy.

Next, the resolution was determined by using the isotopes to produce a measurable peak on the multi-channel analyzer. This peak was then read to fulfill the equation:

$$R = FWHM/H \qquad (2.2)$$

where, R is the resolution, FWHM is the full width at half maximum height of the pulse, and H is the pulse height of the peak.

The detector efficiency was determined to be 90 percent. A measurement of the long term stability of the system is shown in Figure 2.7. In summary since the choice of this gamma-ray spectrometer met all criteria for the experiment, and it had been calibrated properly. The spectrometer was stable for the life of the experiment.

2.4.4 Correction Factors

As with every detection unit certain correction factors must be applied to the data that is measured because of inherent difficulties in the system itself. Since the experimenter cannot be sure that all of

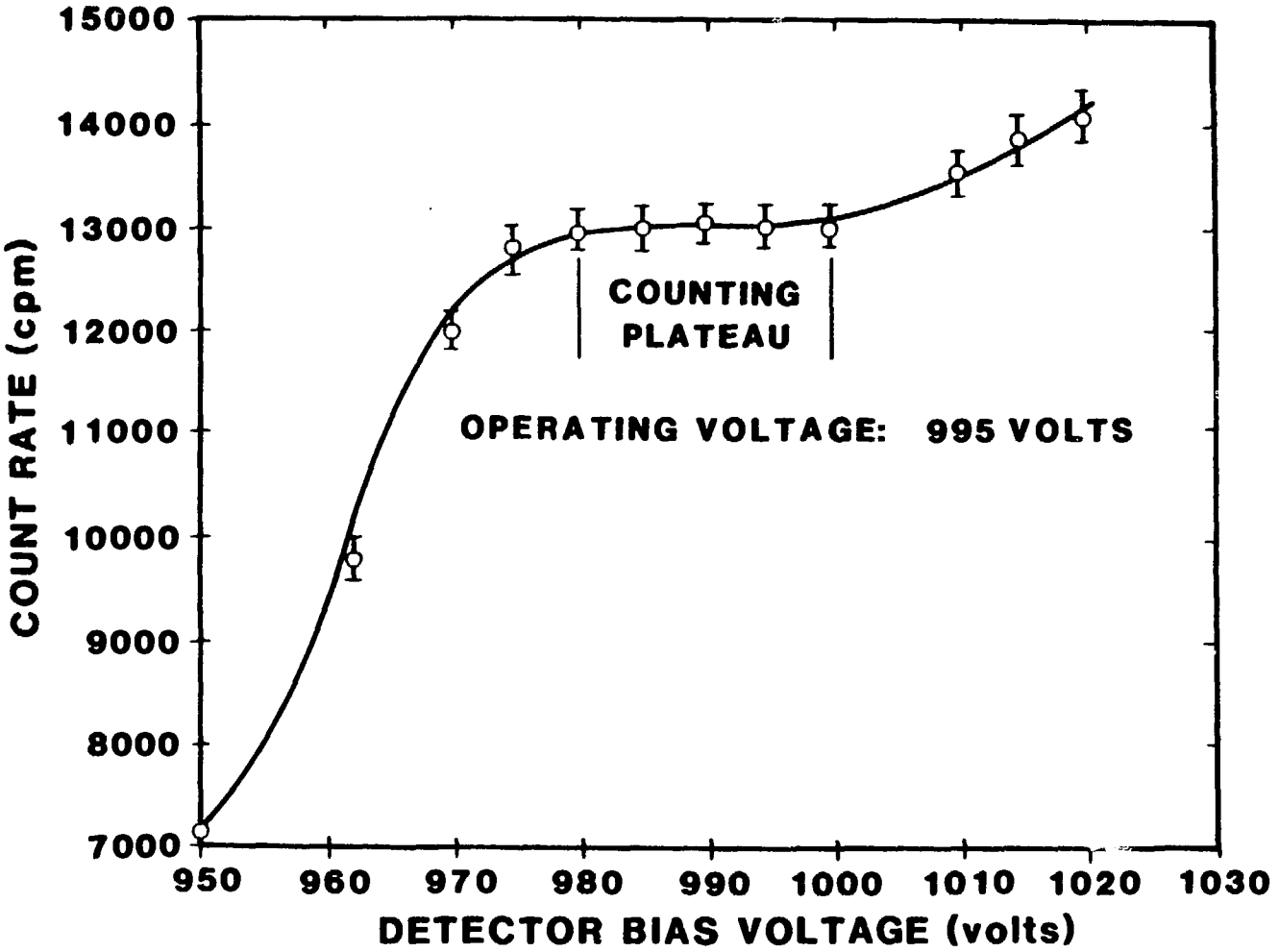

Figure 2.5 Counting Plateau Determination NaI (Tl) Spectrometer
Disc. Bias = 0.1 Volts, Source: Na-22

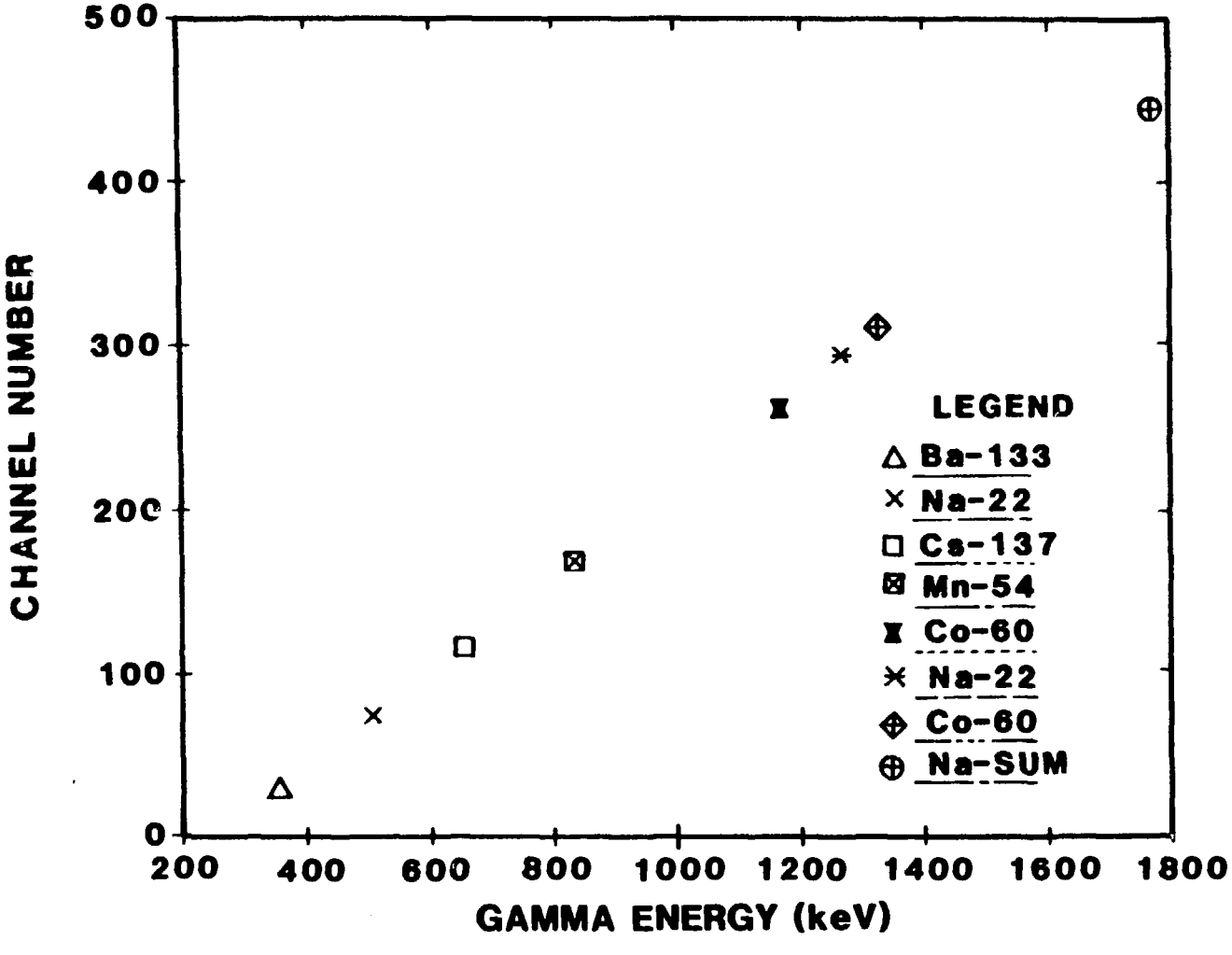

Figure 2.6 Energy Calibration of the Multichannel Analyzer Canberra Series 30 Calibrated Gamma Sources: Ba-133, Na-22, Cs-137, Mn-54, Co-60

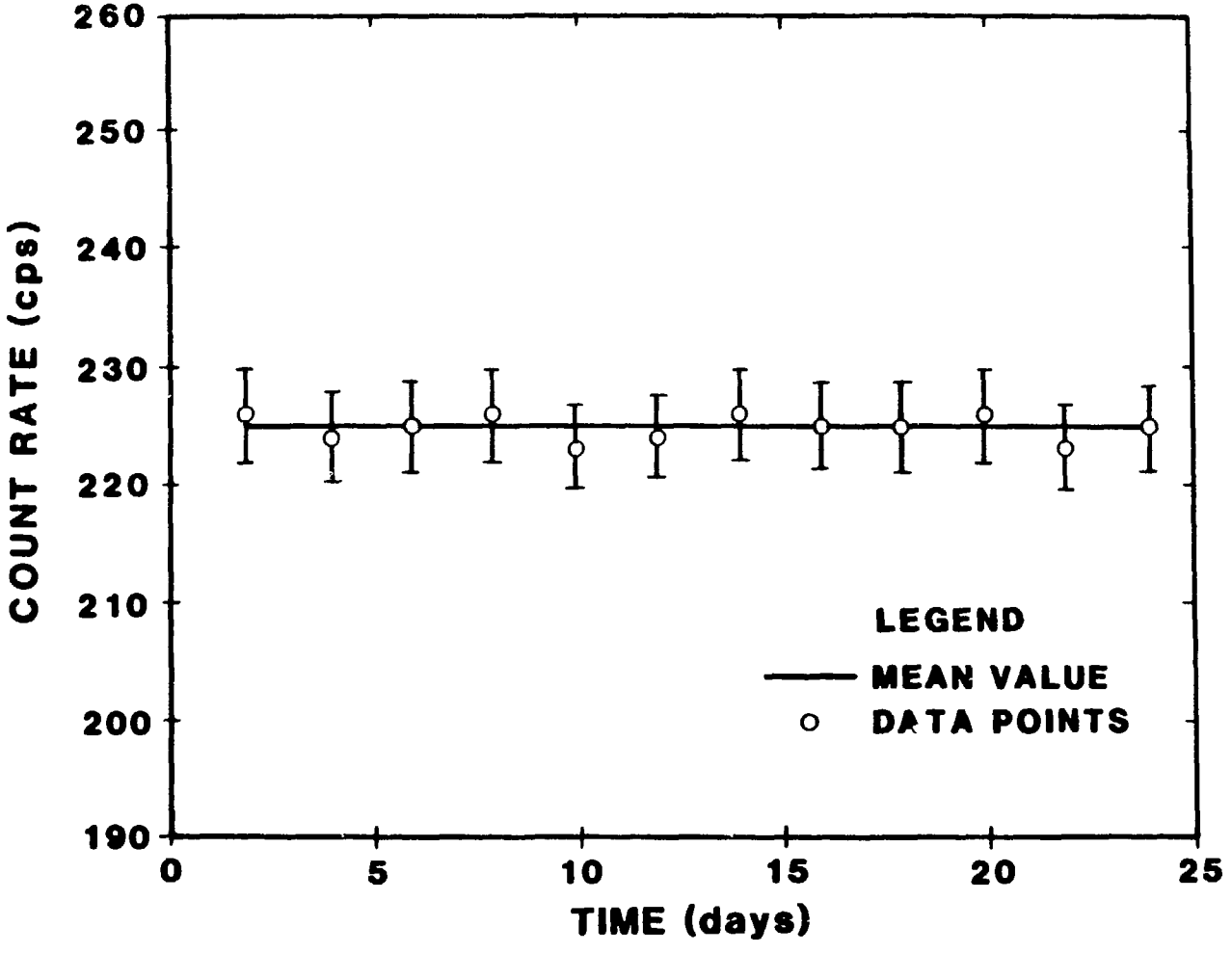

Figure 2.7 Long Term Stability of the NaI (Tl) Spectrometer
Disc. Bias = 0.1 Volts, Source: Na-22

the radiation emitted is actually being measured, certain corrections have been developed to establish the accuracy of the measurement. The resolving time and the chance coincidence rate are two that had to be applied in this detection system.

The resolving time or dead time is the amount of time after an event during which the detector will not respond to another signal. Since the detector cannot always read the pulses as fast as they are emitted, a method was devised to correct for this factor. Although there were several methods for determining the resolving time in a coincidence unit, the method described in Knoll was used in this research [10].

The same Cs-137 source was used for calculating the resolving time. It was placed between the two detectors and the chance coincidence was measured. The Cs-137 emits a characteristic gamma ray at 0.66 MeV. Only one gamma ray is emitted. The source strength was measured for a certain period of time and the single channel count rates and the coincidence count rates are recorded. The resolving time was determined by:

$$r_{ch} = 2\, \tau_{res} r_1\, r_2 \qquad (2.3)$$

where, r_{ch} is the recorded chance coincidence rate, r_1 is the recorded channel 1 count rate, r_2 is the recorded channel 2 count rate and τ_{res} is the calculated resolving time.

By using these calculations, the chance coincidence and the resolving time have been accounted for as correction factors in the gamma-gamma coincidence system. However, the difference in what the detector sees and what radiation is actually emitted must also be accounted for since no system is 100 percent efficient. In order to do this, each detector must first be analysed individually for its efficiency and then

the two together must show some relation in order to find the overall detector efficiency.

Since the radiation emitted from the source occurs simultaneously, the operator has the information needed to establish the absolute source activity or the efficiency of the system. One of the 0.511 MeV photons emitted is recorded by NaI(Tl) number 1, while the other photon emitted in the exact opposite direction at the same time is seen by NaI(Tl) number 2. Since the resolving time is τ, the count rate in number 1 and number 2 can be related as:

$$R_1 = \text{Efficiency}_1 \times N_o \qquad (2.4)$$

and

$$R_2 = \text{Efficiency}_2 \times N_o \qquad (2.5)$$

where, N_o is the true disintegration rate.

Therefore the true coicidence rate measured by the system for this sample is

$$R_C = \text{Efficiency}_1 \ \text{Efficiency}_2 \times N_o \qquad (2.6)$$

Since the coincidence rate can be measured, then the true and the chance coincidence rate can be calculated by:

$$R_{CM} = R_C + R_{Ch} \qquad (2.7)$$

It was also shown that R_C can be calculated with another equation.

Substituting R_C into 2.7, the true coincidence is solved by:

$$N_o = R_1 R_2 / (R_{CM} - R_{Ch}) \qquad (2.8)$$

Therefore the true disintegration rate of the sample has been determined, along with the efficiency of the detector system. It has also been established that the gamma-ray spectrometer meets all of the

criteria for a good detection system to analyze the characteristic radiation emitted from the zinc and copper foils after irradiation.

CHAPTER THREE

EXPERIMENTAL PROCEDURE AND ANALYTICAL METHODS

3.1 Introduction

Since the experimental setup for activation analysis has been delineated in Chapter Two, the analysis of results is the next step in this work. The natural zinc foils were placed at varying distances (5 cm., 10 cm., 15 cm., and 20 cm.) from the target, perpendicular to the beam along with the reference foils. Next, the foils were irradiated for a predetermined length of time, with 14.8 MeV neutrons from the generator. The angle with respect to the beam for the foil placement was zero degrees. In order to measure the ^{64}Zn (n,2n) ^{63}Zn cross section (since ^{63}Zn has a characteristic half life of 38.1 minutes), the reference was the ^{63}Cu (n,2n) ^{62}Cu cross section, where ^{62}Cu has a 9.78 minute half-life, which is reasonably similar to ^{63}Zn for this type experiment. To measure the ^{64}Zn (n,p) ^{64}Cu cross section the ^{65}Cu (n,2n) ^{64}Cu cross section was used as the reference. These two reference cross sections were measured by Ghanbari and Robertson with the exact same experimental set-up [7]. In all cases the foils were not irradiated to saturation because the neutron flux deteriorated severely after a limited amount of time.

Following irradiation, the foils were measured for their radioactive content in the gamma-gamma coincidence system. In addition, to make certain that no impurities contributed to the radioactive content of the isotopes being measured, the decay curves were also plotted and examined

in order to extract the characteristic half-life. Since the ^{64}Cu half-life is 12.71 hours, the researcher needed to wait until the Zn^{63} had decayed away in order get an accurate radioactive content without any ^{63}Zn contributions. This is shown in Figure 3.1, where the two components of the decay curve can be clearly distinguished. Once the saturated activities were determined, the cross sections were calculated by ratioing the saturated activities and multiplying by the reference foil cross section. All other corrections were applied by using the technique developed by Robertson and Ghanbari. The neutron flux was calculated by using the separated isotope as a reference. Since the neutron flux of the Texas Nuclear Neutron Generator was calibrated previously by Ghanbari and Robertson, that step was not repeated for every experiment [4]. Finally, Robertson and Rowland have already shown there is no neutron contribution from scatter within the laboratory [12].

3.2 **Calculations**

Before performing the experiments, it was first necessary to make several calculations, including both macro and microscopic analyses.

To understand the actual cross section calculations, it is imperative to conceptualize the underlying physics of the reactions involved. In general, a nuclear reaction, has the following form:

$$A + B = C + D + \text{del } H \qquad (3\ 1)$$

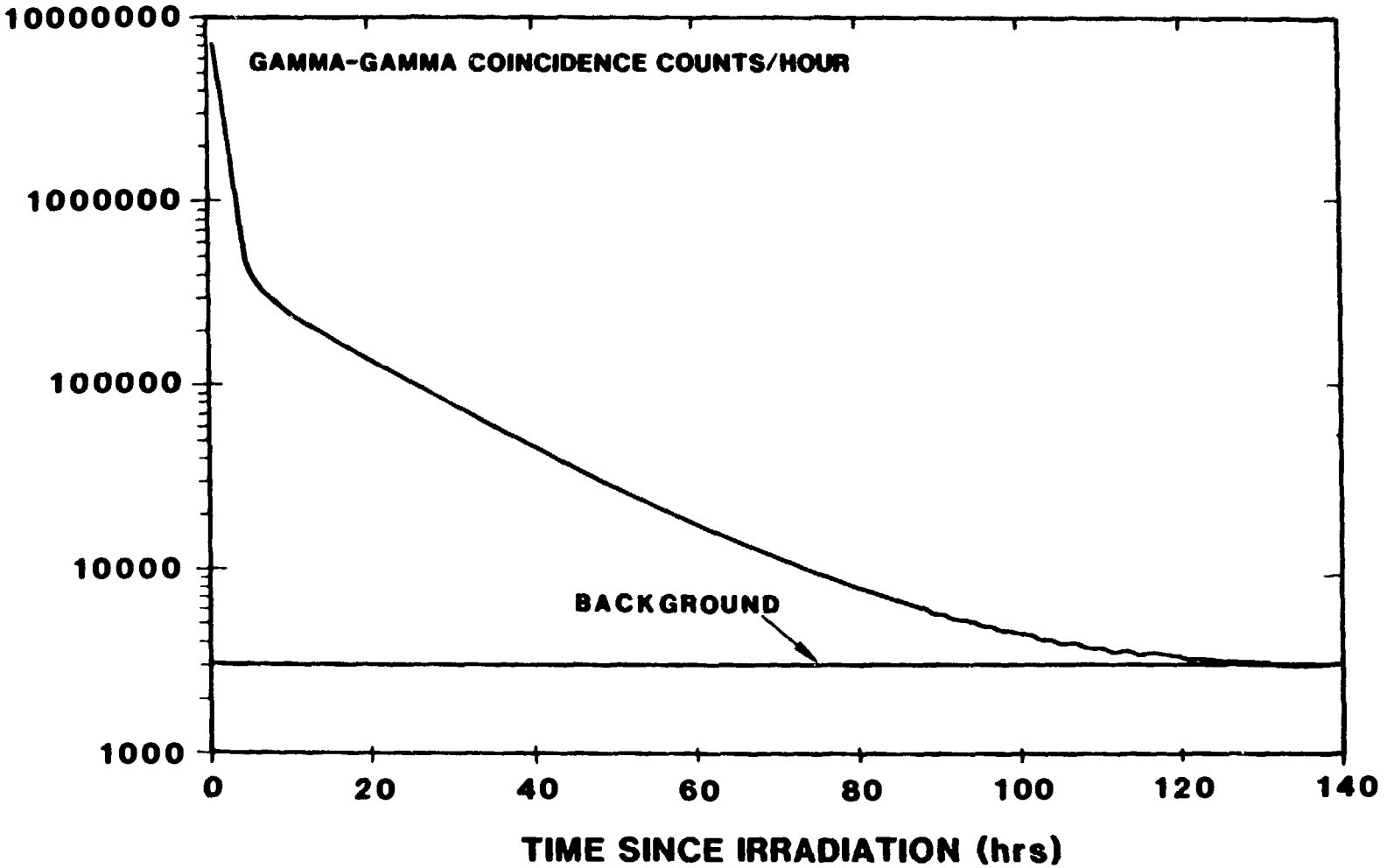

Figure 3.1 Disintegration of Irradiated ^{64}Zn Foil

This equation takes into account the well known conservation of energy. Here, A and B are the reactants, C and D are the products of the reaction and the del H is the energy change of the system. In this experiment, for example, A was the target nucleus, B was the incoming particle, C was the product nuclei, D was the outgoing particle and the change in energy of the system was expressed as Q. In fact, there is a transition system known as the compound nucleus that is the intermediate step between the reactants and the products. This intermediate state exists for 10^{-16} seconds and must be taken into account in any comprehensive nuclear model. With this in mind, then, the reactions that are involved in this experiment can be written:

$$^{64}Zn + \text{neutron} = {}^{65}Zn = {}^{63}Zn + 2 \text{ neutrons} + Q_{(n,2n)} \quad (3.2)$$

and

$$^{64}Zn + \text{neutron} = {}^{65}Zn = {}^{64}Cu + \text{proton} + Q_{(n,p)} \quad (3.3)$$

where ^{65}Zn is the compound nucleus.

Here the neutron produced by the TNNG is the incoming particle and the ^{64}Zn is the target nucleus. The outgoing particles in 3.2 are two neutrons which characterize the reactions that occur at 14.8 MeV. ^{63}Zn is the radioactive product in the first reaction, and ^{64}Cu is the product of the second reaction.

In nuclear physics an important term in determining the energetics of a reaction is the energy change or Q of the reaction expressed in MeV. Q is determined by the mass difference between the initial and final systems, as follows:

$$\text{del Mass (amu)} = M(\text{target}) + M(\text{i.p.}) - M(\text{product}) - M(\text{o.p.}) \quad (3.4)$$

and,

$$Q\ (MeV) = \text{del Mass (amu)} \times 931.4\ MeV/amu \qquad (3.5)$$

The Q values for the reactions are shown in the following Table 3.1:

Table 3.1

Q Values for the Reactions of Interest

Reaction	Q (MeV)
$T(d,n)^4He$	14.1
$^{64}Zn(n,2n)^{63}Zn$	-11.8480
$^{64}Zn(n,p)^{64}Cu$	0.204

Two of the reactions are exothermic; that is, they have a positive Q. There is a net increase in the kinetic energies of the particles. On the other hand, the ^{64}Zn (n,2n) reaction is endothermic (negative Q) and there is a decrease in the energies of the pariticles. These are important concepts because in the exothermic reactions, the nuclear mass is converted into kinetic energy, while in the endothermic reaction the opposite occurs; that is, the kinetic energy is converted into mass.

The threshold energy can be defined as the minimum energy of an incident particle required to produce a nuclear reaction. It is well known that in a exoergic (exothermic) reaction the threshold energy is zero. On the other hand the threshold for the endothermic ^{64}Zn $(n,2n)^{63}Zn$ reaction is 12.048 MeV.

3.2.1 Saturated Activity Determination

Once it has been established that the reaction can take place at a given neutron energy, the next step is to examine what happens when a target is irradiated by 14.8 MeV neutrons.

First, it is important to recognize that when the neutrons interact with the target ^{64}Zn a certain amount of the ^{63}Zn or ^{64}Cu is produced as a function of time. This production is defined as the reaction rate,

$$RR = dN_p /dt \qquad (3.7)$$

where, N_p is the number of nuclei produced in the change of the time dt, or in terms of the neutron flux produced by the generator by:

$$RR = n \sigma \Phi \qquad (3.8)$$

where, σ is the reaction cross section (cm^2), n is the number of atoms in the target, and Φ is the flux of the neutrons (particles/cm^2-second).

It is well known that the rate of change of the product nuclei during the irradiation is the difference between the production rate and the decay rate. Even though the main concern of the experiment is to produce radioactive nuclei, it should be remembered that even as nuclei are being produced some are decaying at the same time. The simultaneous phenomena may be expressed by:

$$D_p = \lambda * N_p = RR(1 - e^{-\lambda * t}) \qquad (3.9)$$

where, D_p is the decay rate of the product nuclei, N_p is the number of nuclei produced, and λ is the decay constant for the isotope of interest.

The saturated activity is obtained when the decay rate approaches the production as a limiting value, essentially when the decay rate is equal to the production rate. This is usually assumed to occur after irradiation for approximately 5 half-lives. In the case of the TNNG the flux is reasonably constant for a limited period of time. Therefore, the analyst must choose a happy medium between good irradiation time and statistically valid flux variation. Along with the irradiation time, another important factor in determining the saturated activity is the fact that for long-lived product radionuclides irradiation time is essentially a linear function of the mimimum amount of radioactivity desired. Therefore, saturated activity which has importance for this research depends upon three factors, 1) the half-life, 2) statistical accuracy and 3) neutron flux steady state operating time of the Texas Nuclear Neutron Generator. The results of the applications of these three factors are presented in Chapter Three.

Not only does the saturated activity play an important role in the irradiation time, but it also plays the key role in the determining the cross section, because the ratio between the saturation activity in the reference foil and the target foil multiplied by the reference cross section determines the product nuclei cross section.

Because it was not possible to irradiate the foils to full saturation, an alternative method was used to determine the saturated activity. The saturated activity was calculated by the same method used by Robertson and Ghanbari [4]:

$$A_{sat} = A_{irr}/(1-e^{-\lambda t_{irr}}) \qquad (3.10)$$

and the activity of each foil was calculated using the measured absolute activity at the end of irradiation period:

$$A_{irr} = \lambda * N_o / [e^{-\lambda\ tw} - e^{-\lambda\ (tw + tc)}] \qquad (3.11)$$

where, tw is the time period recorded between the end of the irradiation period and the beginning of the counting period, λ is the decay constant of the product isotope, tc is the counting period, and N_o is the calculated total count for the counting period denoted by tc.

3.2.2 **Cross Section Determination**

The target material for this experiment was natural zinc metal in the form of a foil. Natural zinc metal is composed of three separate isotopes: ^{64}Zn, ^{66}Zn and ^{68}Zn. For the purpose of this experiment, only ^{64}Zn was analyzed. The isotopic abundance of ^{64}Zn is 48.6 percent.

As presented in the last chapter, the N_o or the true disintegration rate corresponds to the saturation rate. Consequently, the true disintegration rate can be determined once the saturation rate is known because, essentially, one depends upon the other. It has already been evaluated that the basis of the true disintegration rate is obtained from the expression [7]:

$$N_o = [N_1\ N_2 / N_C]\ (\Phi_1 + \Phi_2 / [(1 + \Phi_1)\ (1 + \Phi_2)]) \qquad (3.12)$$

where,

N_1 is the number of counts in channel one, $N_2$is the number of counts in channel two, and N_C is the number of counts in the coincidence channel. Φ_1 and Φ_2 are the relative efficiencies of the individual NaI crystals to the gamma radiation being measured. Since both of the crystal detectors receive the same energy gamma radiation (0.511 MeV), the efficiencies are equal. Therefore, the above equation becomes

$$N_o = N_1 N_2 / N_C \qquad (3.13)$$

As was stated previously, the angular correlation and the source detector geometry factor do not enter into the calculations because the previous conditions apply [7]. These are a) the two gamma rays have the same energy and are emitted in exactly opposite directions; and b) the distance between the source and the detector are equal and this distance is very much smaller than the radius and the thickness of the Na(Tl) crystals; and c) the angle between the longitudinal axes of the detectors is 180^o.

In this research the above equation was modified for the background, dead time and the previously calculated resolving time. The equation then becomes

$$N_o = \frac{(N_1 - N_{b1})(N_2 - N_{2b})}{2\,(N_C - N_{Cb})} \quad (1 + \tau_{res})\left(\frac{N_1 N_2}{N_C}\right) \qquad (3.14)$$

where N_{1b} is the background in channel one, N_{2b} is the background in channel two, and N_{Cb} is the background in the coincidence channel.

The previously delineated saturated activity is calculated by accounting for the correct matrix percentage, isotopic mass and mole fraction in that sample.

3.2.3 **Decay Scheme Determination**

Once the saturated activity has been determined, certain correction factors must be considered to find the real activity. First, the

branching ratio must be considered because the nuclear constants that are determined by it are the decay scheme and the half-life and are of primary importance here. Decay schemes played an important role in this work because the decay scheme affects the quantitative determination of positron emission with subsequent annihilation radiation. Since a radioistope source can decay in many ways, the decay scheme becomes a diagnostic tool for the experimenter. Because of the correlation between the energies of the positron particles and the gamma rays, it is possible to construct a nuclear energy diagram for the radioisotope of interest. This is called the decay scheme.

The decay schemes for ^{63}Zn, ^{64}Cu and ^{62}Cu are shown in Figures 3.2, 3.3, and 3.4. The diagonal lines represent the different beta particles and the vertical lines represent the gamma rays that are also experimentally determined. However if no gamma ray is emitted, then the beta transition is directly to the ground state. It is interesting to note that the ^{64}Cu decay scheme exhibits all three types of beta decay: electron capture, positron emission, and electron emission. It should also be noted that without accurate determination of the branching the cross section could not accurately be determined since it depends upon a very accurate branching ratio. In contrast to ^{64}Cu, ^{63}Zn does not exhibit a variety of beta decay, because it exhibits only electron capture and positron emission. In 1983 Christmas and Reyes reexamined the decay scheme for ^{64}Cu with confidence limits in the 99 percentile [13]. Thus, the decay scheme is known very accurately. On the other hand, the decay scheme for ^{63}Zn has not been accurately reevaluated for forty years. Therefore, the error in this determination is ten times

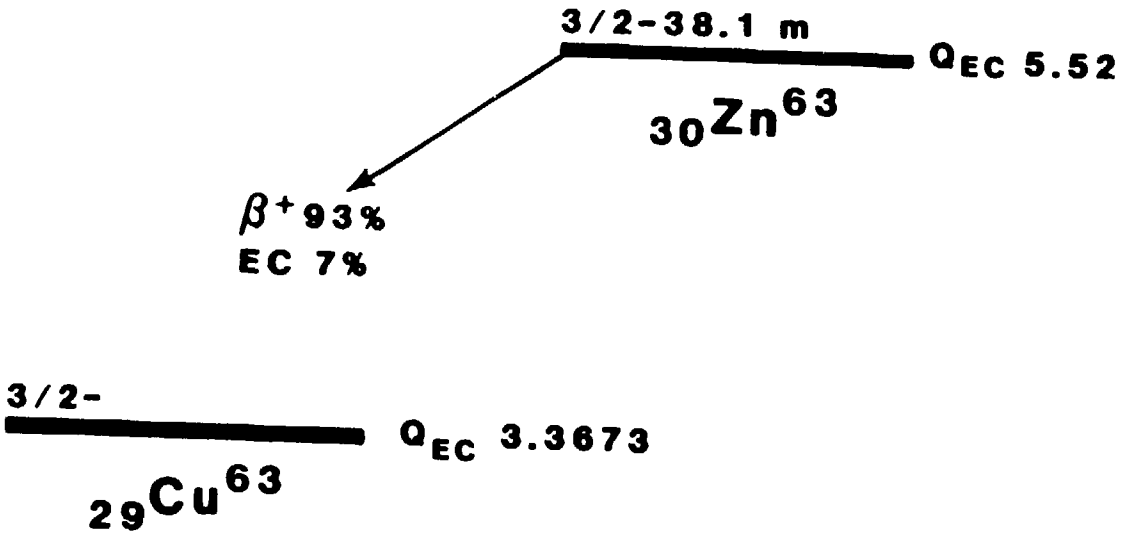

Figure 3.2 Decay Scheme of ^{63}Zn

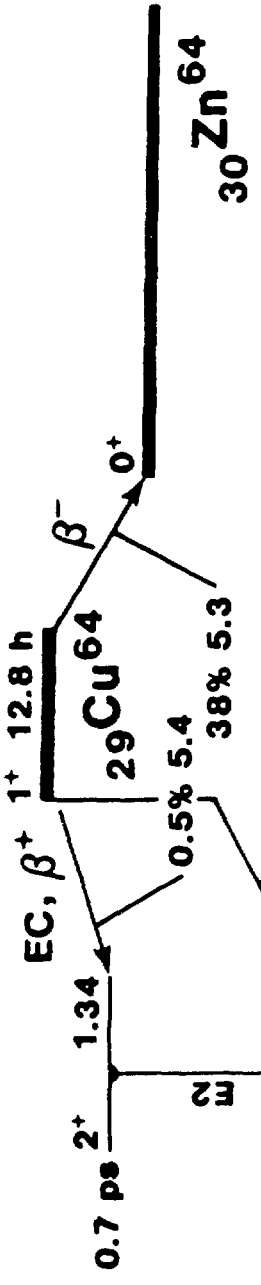

Figure 3.3 Decay Scheme of $_{29}Cu^{64}$

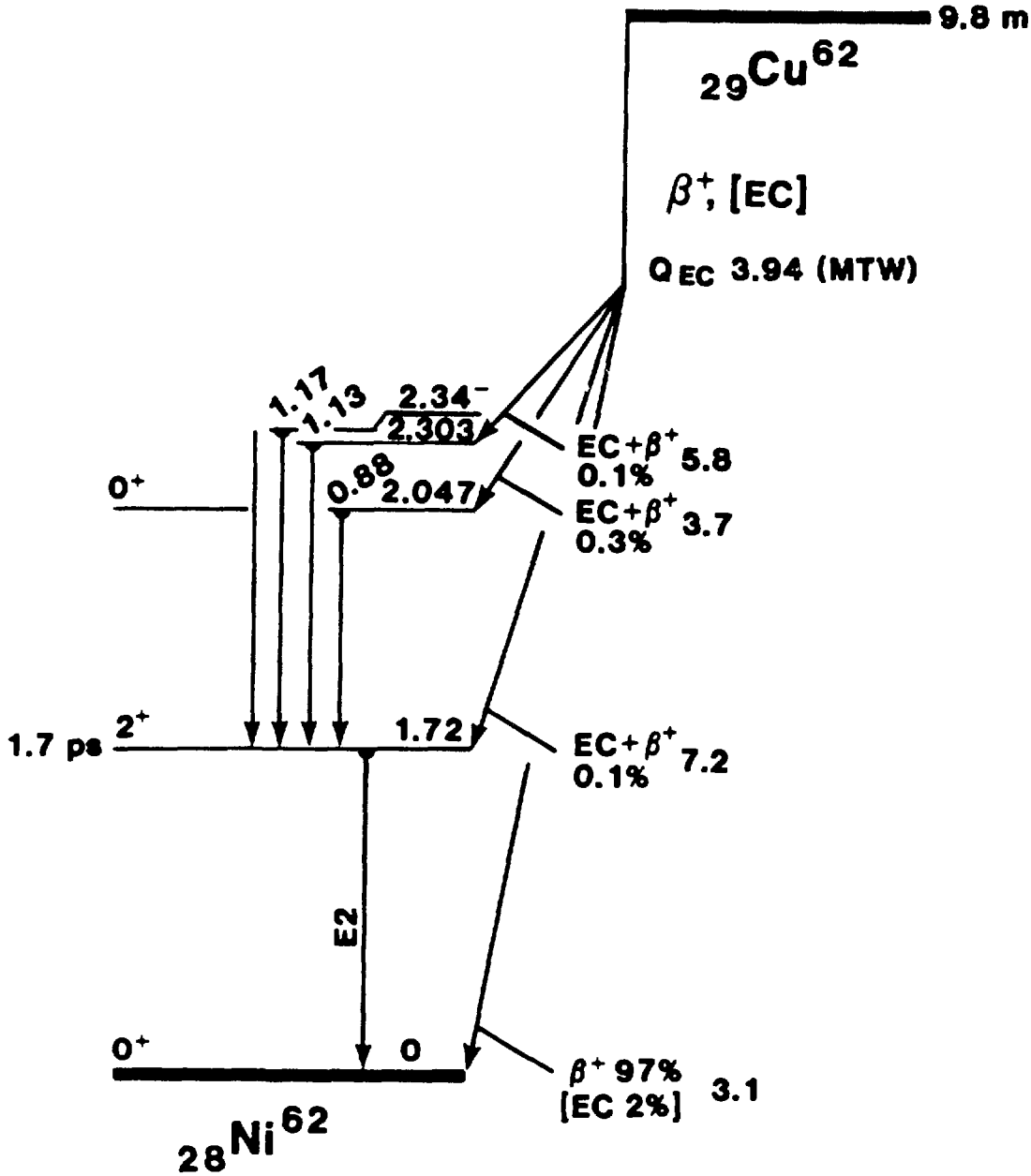

Figure 3.4 Decay Scheme of $_{29}Cu^{62}$

greater than that of the ^{64}Cu decay scheme. Thus, a reevaluation of the decay scheme needs to be performed.

Next, the cross-section that is being used as the reference cross section must be analyzed for the uncertainty associated with its measurement. Finally, the ratio of the corrected activities multiplied by the reference cross section (σ) gives the final cross section of interest, thus producing the activation cross section.

This is given by the following equations:

$$\sigma_1/\sigma_2 = (A_{sat\text{-}1} / A_{sat\text{-}2}) * (M_1 / M_2) \qquad (3.15)$$

where, M_1 and M_2 are the atomic weights of the elements 1 and 2, respectively.

The results of the these corrections and equations are presented in Chapter Five.

CHAPTER FOUR

THEORETICAL CALCULATIONS AND MODELS

4.1 Introduction

Theoretical cross section calculations for the ^{64}Zn (n,p) ^{64}Cu and the ^{64}Zn (n,2n) ^{63}Zn reactions were performed using the Los Alamos reaction theory code GNASH[6]. Also calculated were ^{63}Cu (p,n) and ^{65}Cu (p,n) cross sections to validate the proton optical model used for the code, as well as other n + ^{64}Zn reactions that compete with the (n,p) and (n,2n) reactions.

Since many papers on theoretical calculations with GNASH and similar codes exist in the literature, the reader is referred to earlier work for a detailed description of the theory [14]. Certain aspects of the calculations, however, will be highlighted here, including an overall description of the GNASH code. Detail is also given to the Hauser-Feshbach statistical model as well as to the optical model, which provide the foundations for the theoretical calculations.

4.2 GNASH

The theoretical cross sections of this work were calculated using the GNASH reaction theory code in collaboration with Phillip G. Young in the group T-2 at Los Alamos National Laboratory. The code is a pree-quilibrium, statistical model that is based on Hauser-Feshbach

statistical theory [6]. With such an approach, one is able to calculate cross sections for several reactions such as the (n,2n), (n,p), (n,n'), etc. What is unique about the code is that each calculation can track decay sequences of a target nucleus with 10 or more compound nuclei, and the compound nucleus can emit up to six different types of radiation.

The reactions calculated here are depicted schematically in Figure 4.1. Neutrons incident on ^{64}Zn form the main compound nucleus ^{65}Zn which subsequently decays by emission of neutrons, gamma-rays, protons and alphas. Each significant residual nucleus that is formed can decay by the same types of emission. The code tracks the populating of individual states in each nucleus as well as the emission spectra for each chosen radiation. Conservation of angular momentum and parity are included explicitly. For these calculations the incident particles were neutrons, but one can also use protons, deuterons, tritons and ^{3}He or ^{4}He particles. Thus, the code provides the maximum flexibility not only for the emitted particles, but also covers a gamut of incident particle types.

However, in order to run the code, several types of input must be predetermined. Most importantly, suitable optical model potentials must be determined in order to provide GNASH with particle transmission coefficients. In this work, the SCATOP2 code was used to obtain a neutron optical model potential by fitting the published experimental data [15]. A companion code, SCAT86, was then used to calculate the optical model transmission coefficients.

The level structural information for the nuclei to be calculated must also be determined for input into the code. Experimental data exist in the Table of the Isotopes for low-lying discrete levels [16].

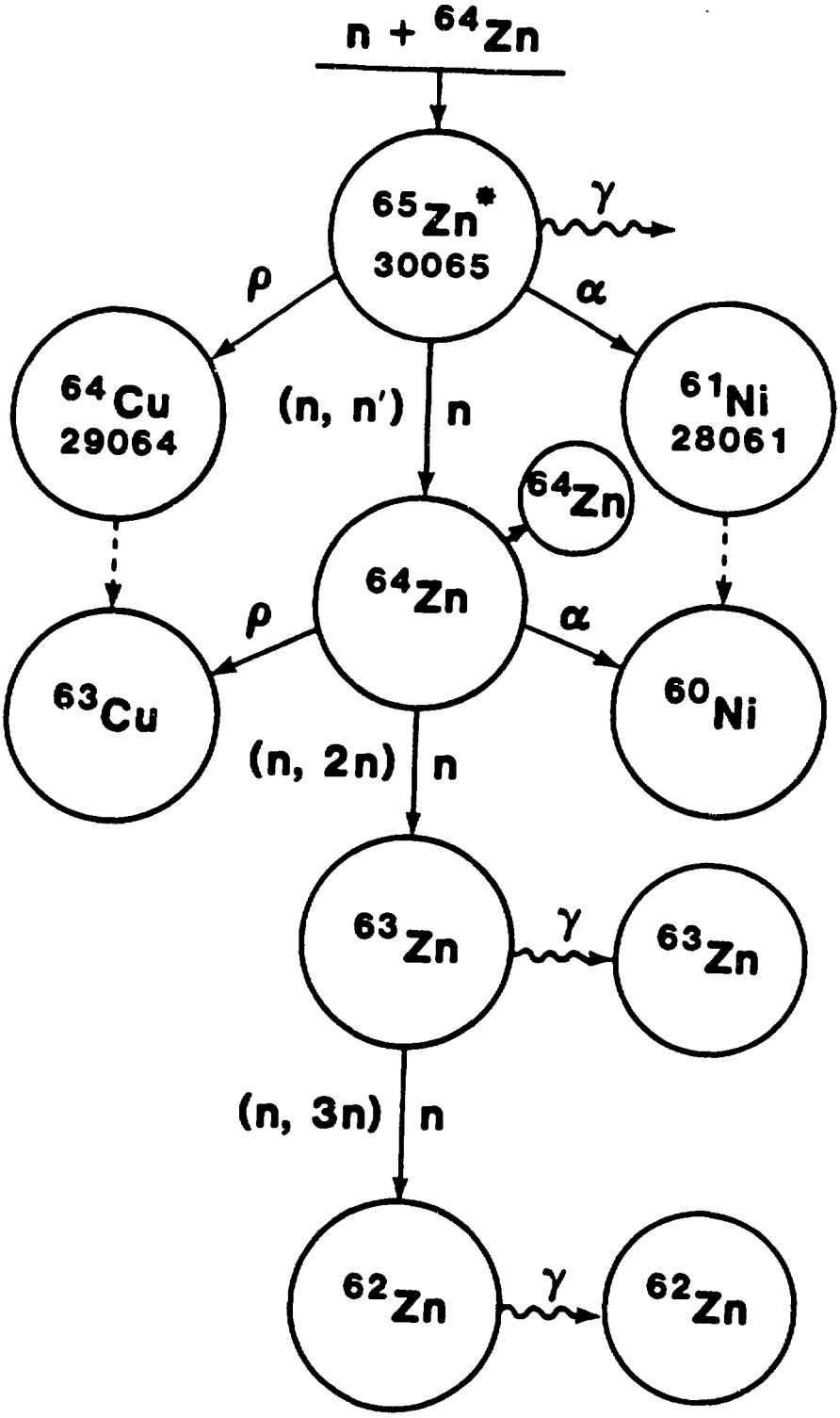

Figure 4.1 Sample Decay Chain for GNASH Calculations

Although the levels that have not been observed above some cutoff energy must be theoretically calculated, and are represented in terms of level densities (number of levels per unit energy). These are calculated in GNASH from the expressions by Gilbert and Cameron [17]. At lower excitation energies the level densities are calculated by assuming a constant temperature expression and matched to the experimentally determined region, as illustrated schematically in Figure 4.2. At higher excitation regions the Fermi-gas form is used to calculate the level densities, appropriately matched to the constant temperature level densities. GNASH has an option for doing all matching internally during a calculation, and this option was utilized. However, it was necessary to provide experimental information on the low lying discrete levels as input and to predetermine exactly which levels and excitation energies were matched with the Gilbert and Cameron constant temperature expression.

As a "First Pass" in running the GNASH code, no correction was made for direct reaction effects on the cross section calculations. The results, however, were found to underpredict the (n,n') cross sections that compete with the (n,p) reactions in the MeV region. Therefore, the final approach taken was to use the code DWUCK to calculate direct reaction cross sections for combination with the compound nucleus/preequilibrium results from GNASH [18]. DWUCK uses the Distorted Wave Born Approximation, along with the neutron optical model parameters, to determine relative direct cross sections for inelastic scattering. Absolute values were determined by using experimental ^{64}Zn (p,p') results for the deformation parameter ($beta_\ell$). While the direct

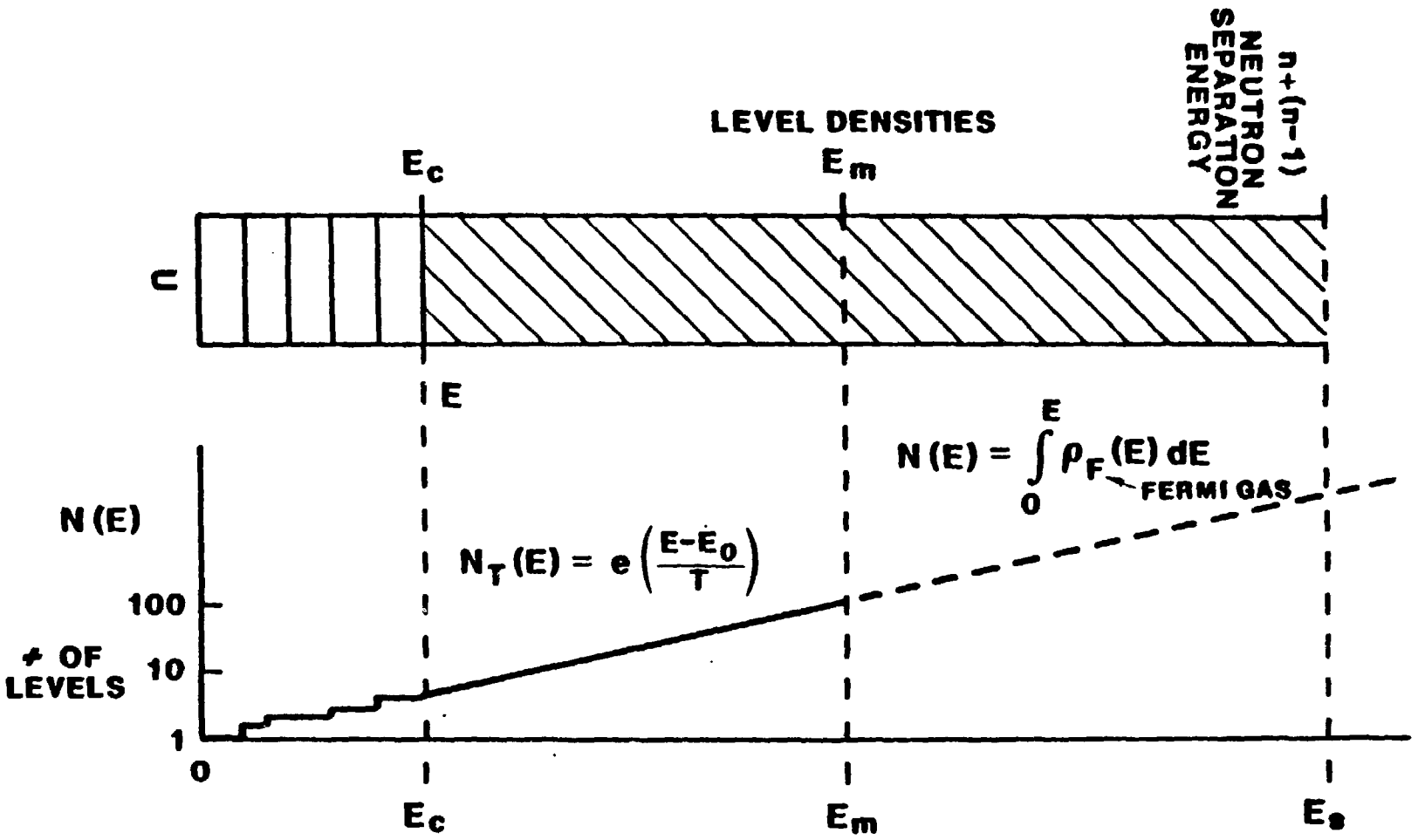

Figure 4.2 Schematic Representation of Level Densities over the Experimental, Temperature and Fermi Gas Regions

reaction results only indirectly affected the (n,p) and (n,2n) calculations, they did improve agreement with the experimental data somewhat in the 14 MeV energy region, and markedly improved the agreement in the low energy region. Addition of the direct effects changed the (n,p) cross section by 7 percent and the (n,2n) cross section by 12 percent at 14.8 MeV, both in the direction of improving agreement with the measurement.

Width fluctation corrections were made primarily to improve the calculations at lower energies [6]. Additionally, the preequilibrium correction was adjusted to give a preequilibrium fraction of about 25 percent at 14.8 MeV. It has been learned from previous analyses involving other nuclei that a preequilibrium ratio of this magnitude accurately (≈10 percent) reproduces measured neutron emission spectra. Since experimental data were measured only at 14.8 MeV, data at other energies were obtained from the National Nuclear Data Center at Brookhaven National Laboratory for comparison with the calculations [19]. A schematic illustration of the calculational scheme for GNASH is shown in Figure 4.3.

4.3 Hauser-Feshbach Statistical Model

The Hauser Feshbach statistical model describes reactions in medium weight nuclei by light, fast particles [20]. It is also a model that allows for the conservation of angular momentum of the interacting particles. It is important to remember that the compound nucleus is the apex of the model, for it is around the compound nucleus that the model is constructed. In the present work the compound nucleus is formed when

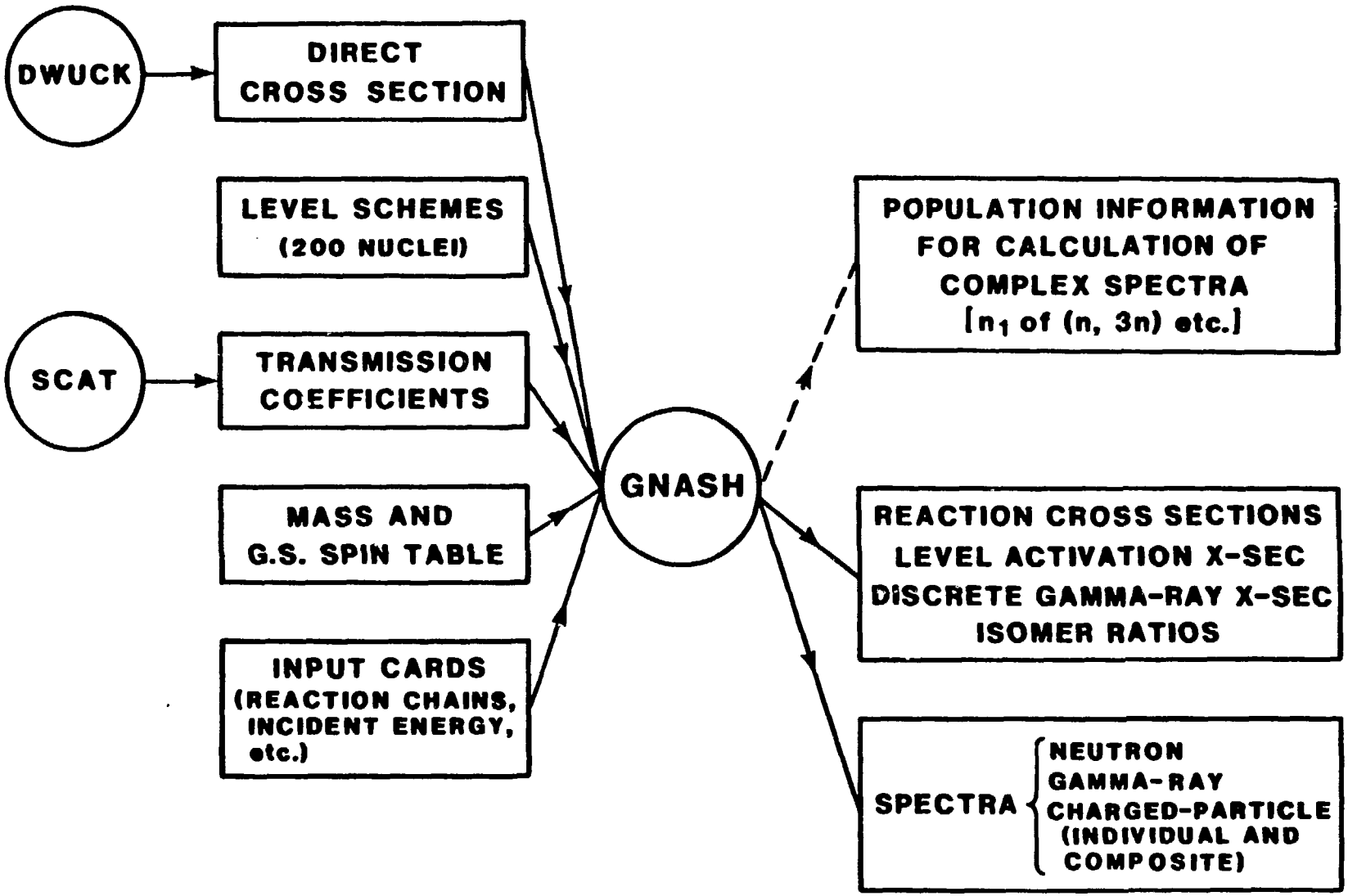

Figure 4.3 Schematic of Calculated Scheme

the neutron interacts with the ^{64}Zn to form ^{65}Zn. Although the compound nucleus only lasts 10^{-16} seconds, it can have a large cross section. Consequently the central question is: What is the probability for the formation of the compound nucleus and for its decay into particular states? The formation and disintegration of the compound nucleus are the two stages of this model, and both stages conserve energy (E or U), spin (J) and parity (Π) [21].

A schematic illustration of the formation and decay of the compound nucleus is given in Figure 4.4. The basic equations which describe these quantum terms are:

$$\epsilon + B_a = \epsilon' + E' + B_{a'} = U \qquad \text{Energy} \qquad (4.1)$$

$$\vec{I} + \vec{i} + \vec{l} = \vec{I}' + \vec{i}' + \vec{l}' = \vec{J} \qquad \text{Angular Momentum} \qquad (4.2)$$

$$p * P * (-1)^{l} = p' * P' * (-1)^{l'} = \Pi \qquad \text{Parity} \qquad (4.3)$$

where, ϵ and ϵ' represent the center-of-mass kinetic energies of the incoming and outgoing light particles (a and a'), E' is the excitation energy of the residual nucleus, and B_a and $B_{a'}$ are the particle binding energies relative to the main compound nucleus. The excitation energy, total angular momentum, and parity of the main compound system are denoted by U, $\vec{J}$, and Π, respectively. The quantities $\vec{i}$ and $\vec{I}$ represent the spins of the light and heavy particles, p and P are the parities, $\vec{l}$ is the orbital angular momentum, and the primes indicate the outgoing channel.

For the present problem, the compound nucleus can emit gamma rays and three types of particles: neutrons, protons and alphas. The gamma ray emission is described in section 4.8.

BASIC HAUSER-FESHBACH EQUATIONS

ENERGY: $\epsilon + B_a = \epsilon' + E' + B_{a'} = U$

ANGULAR MOMENTUM: $\vec{I} + \vec{i} + \vec{l} = \vec{I}' + \vec{i}' + \vec{l}' = \vec{J}$

PARITY: $p \cdot P \cdot (-1)^l = p' \cdot P' \cdot (-1)^{l'} = \pi$

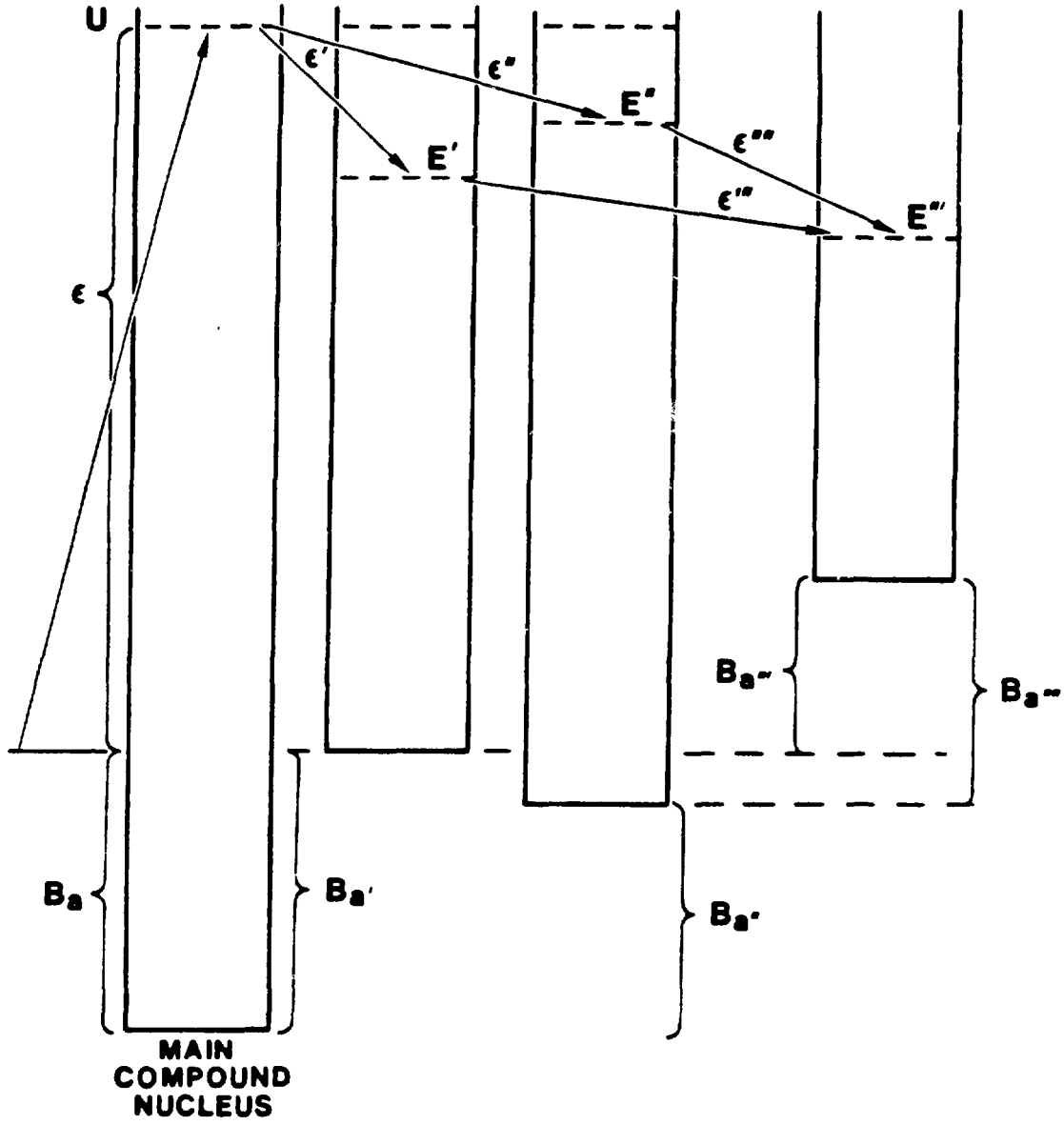

Figure 4.4 Schematic Illustration of the Formation and Decay of the Compound Nucleus

The compound nucleus cross section can be determined in terms of transmission coefficients, T_ℓ, which can be defined simply as the probability of penetration of a potential barrier by the emitted particle. Transmission coefficients can be calculated from an optical model, which is described in section 4.6. The compound nucleus formation cross section is related to the transmission coefficients by the expression:

$$\sigma_a(E,I,P;U,J,\Pi) = (\pi/k^2)[\ (2J+1)/(2i+1)(2I+1)] * \sum_{S=|I-i|}^{I+i} \sum_{\ell=|J-S|}^{J+S} f\ (\ell,\Pi)\ T_\ell^a\ (\epsilon) \qquad (4.4)$$

where

k = the wave number of the system,

$\sum_\ell \sum_S$ = sum over spin and angular momentum.

The above formalism is in GNASH, and σ_{cn} is determined by the T_ℓ that are input into the code. Decay calculations of the compound nuclei are also carried out in GNASH. The cross section for forming a final state b of a specific spin and parity from an intial state a is given by:

$$\sigma_{a,b'} = \sum_{J\Pi} \sigma_{cn}(\epsilon,I,P;\ U,J,\Pi)\ \Gamma_b'\ (U,J,\Pi;E',I',P')/\Gamma\ (\ U,J,\Pi) \qquad (4.5)$$

where

$\sum_{J\Pi}$ = the sum over angular momentum and parity of the compound states that are consistent with with initial and final states

σ_{cn} = compound nucleus cross section

Γ_b' = the decay width for the compound nucleus into a state in the residual nucleus by emission of particles b.

Γ = the total decay width. This includes all particles whose emissions are possible and is obtained by summing Γ_b' over all final states and particles.

The decay widths for particles, Γ_b', are calculated from the reciprocity theorem for nuclear reactions as follows:

$$\Gamma_b'(U,J,\Pi;E',I',P') = \mu\epsilon(2i'+1)(2I+1)/[(\pi\hbar)^2(2J+1)\rho(U,J,\Pi)]* \sigma_{b'}^{inv}(E',I',P';\ U,J,\Pi) \qquad (4.6)$$

where

μ = reduced mass of the residual system,

ϵ = decay energy,

σ_a^{inv} = cross section for the inverse compound nucleus reaction,

ρ = level density of the intermediate nucleus.

The inverse reaction cross section can then be expressed in terms of transmission coefficients as shown in:

$$\Gamma_b'(U,J,\Pi;E',I',P') = [1/[2\pi\rho(U,J,\Pi)]]\sum_{S=I'-I}^{I'+P-i'}\ \sum_{I=J-S}^{J+S} f(\ell,\Pi) * T_\ell^{b'}(U-E'-B_a) \qquad (4.7)$$

where h is Planck's constant.

A new concept, that of the level density, has now been introduced. As the excitation energy of a nucleus increases, the detailed level information disappears. Therefore, to account for the level information that is needed, the concept of a level continuum, given by a smooth function specifying the number of levels of given J, Π, per unit energy, is introduced. This representation leads to the following expression for the total decay width by a particle from a compound state of given spin and parity:

$$\Gamma(U,J,\Pi) = \sum_{a}\sum_{I}\sum_{P} \int_{E_g}^{U-B_a} dE\ \Gamma_a(U,J,\Pi;E,I,P)\rho(E,I,P) + \Sigma_k \Gamma_k(U,J,\Pi;E_k,I_k,P_k)$$

(4.8)

where, E_G is the maximum excitation energy of discrete states in the residual nucleus and k is summed over its discrete states.

4.4 Level Density Model

Nuclear level densities have been analyzed by Gilbert and Cameron [17]. As illustrated earlier, there are three regions in the level density model: the first region contains the discrete energy (experimental) levels; the second region is the temperature dependent continuum region; and the third region is the Fermi gas continuum region. In order to calculate the level densities in the continuum region, certain experimental data on low-lying levels from Table of the Isotopes must be given to the model [16]. The temperature region in the model is then matched to these experimental data as well as to the Fermi gas region at higher excitation energies. See Figure 4.2 for a schematic representation of the complete level density region. The actual fitted level information used in the calculation is seen in Figures 4.5 - 4.11.

In general, the level density for the nucleus can be represented as:

$$\rho(J,\Pi,E) = F_{\Pi}(\Pi)F_j(J,E)\rho(E) \qquad (4.9)$$

where,

E = nucleus' excitation energy,

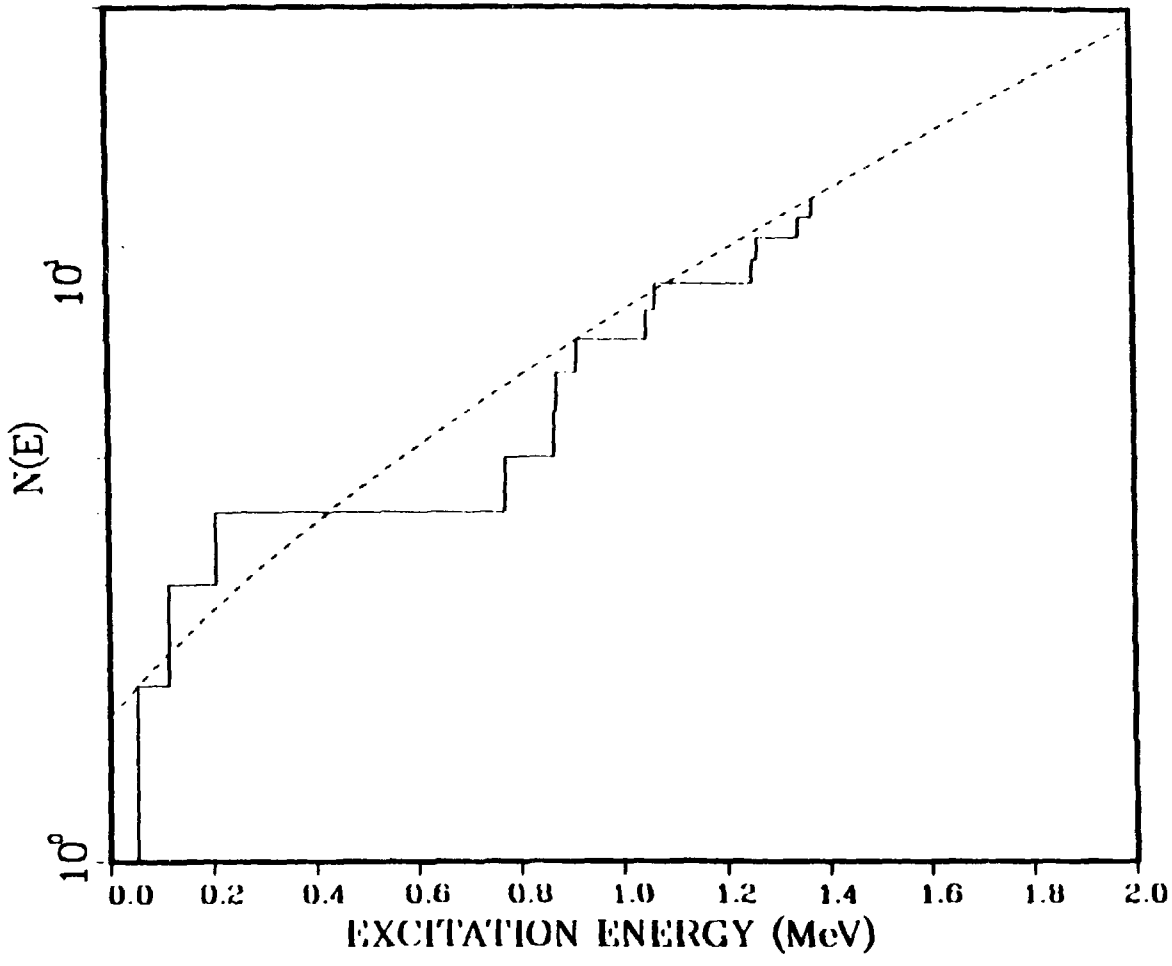

Figure 4.5 Experimental Levels and Level Fit of ^{65}Zn

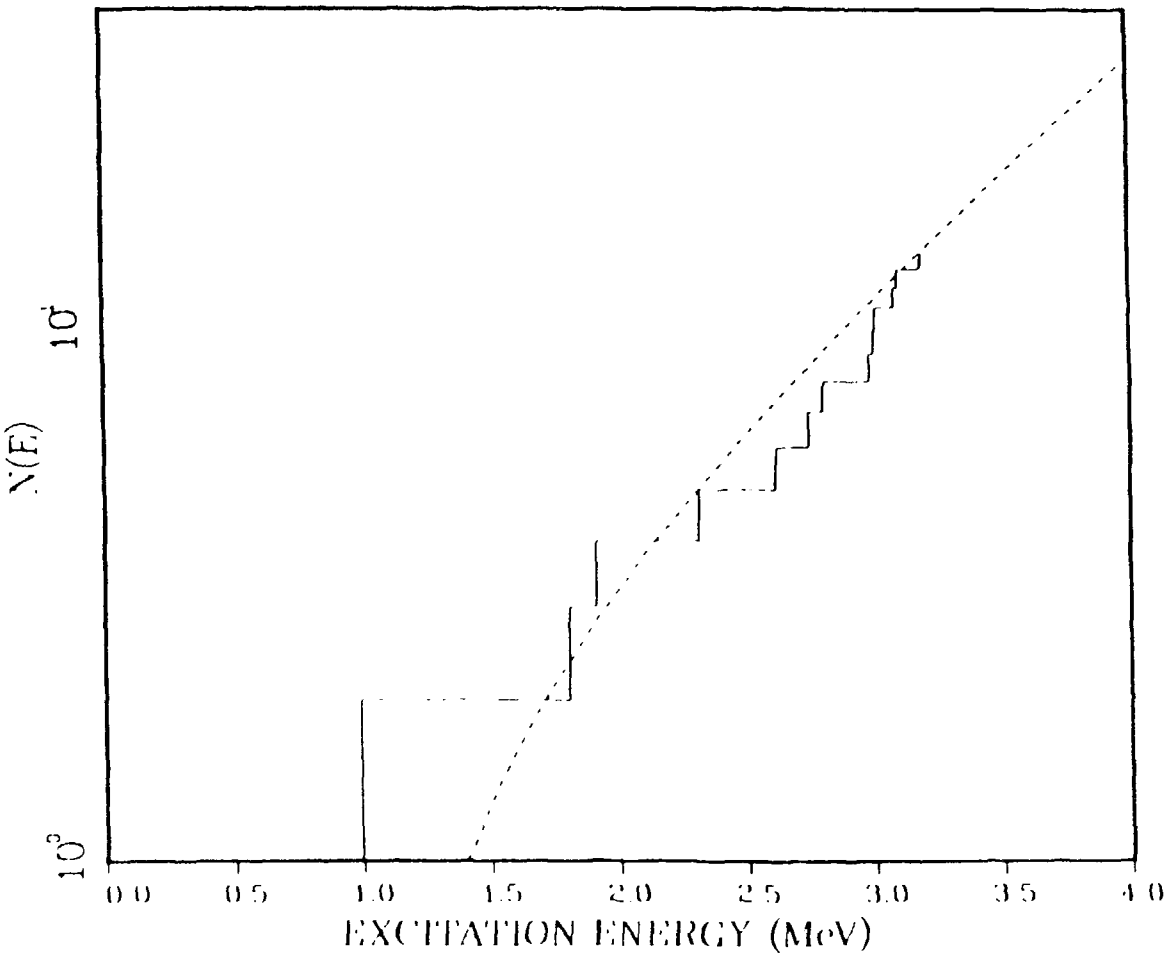

Figure 4.6 Experimental Levels and Level Fit of ^{64}Zn

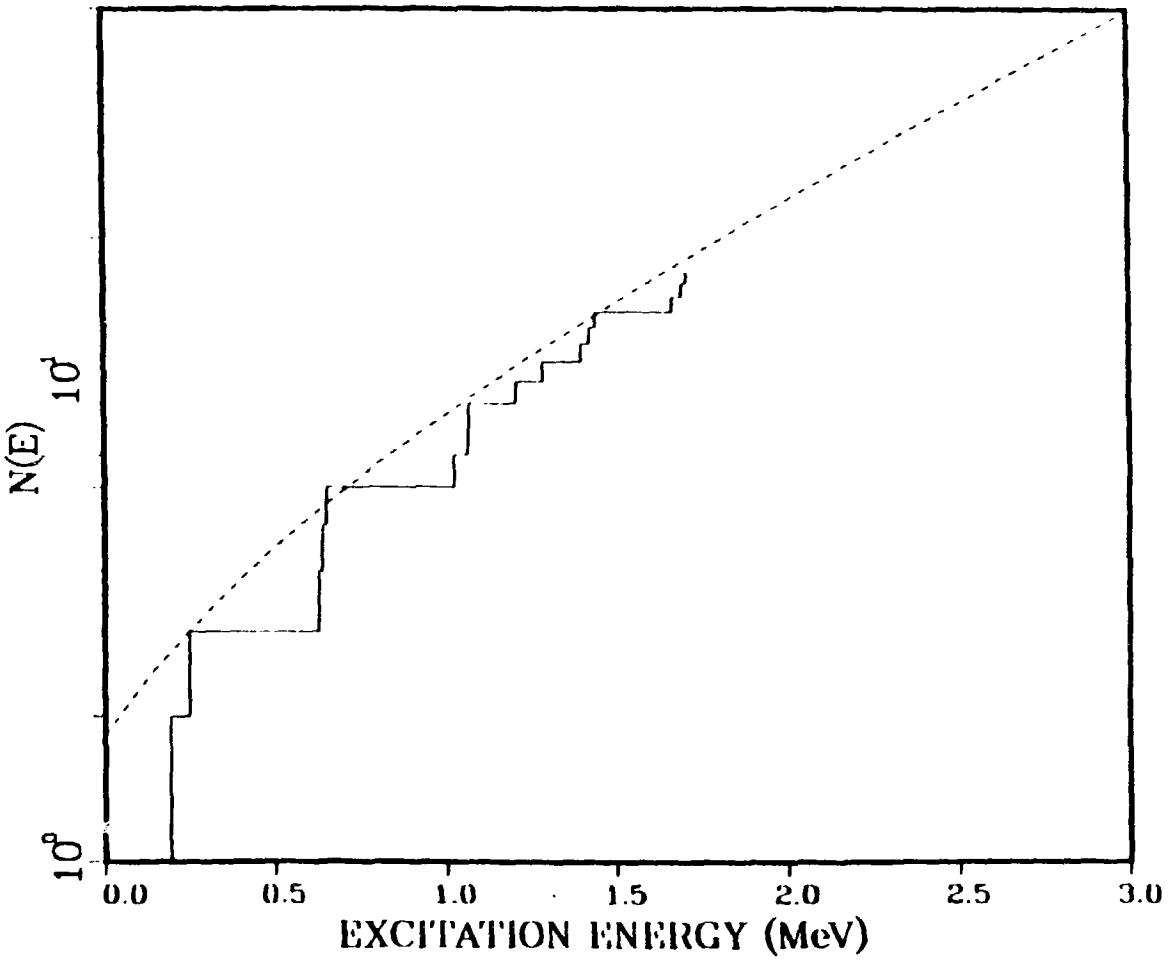

Figure 4.7 Experimental Levels and Level Fit of ^{63}Zn

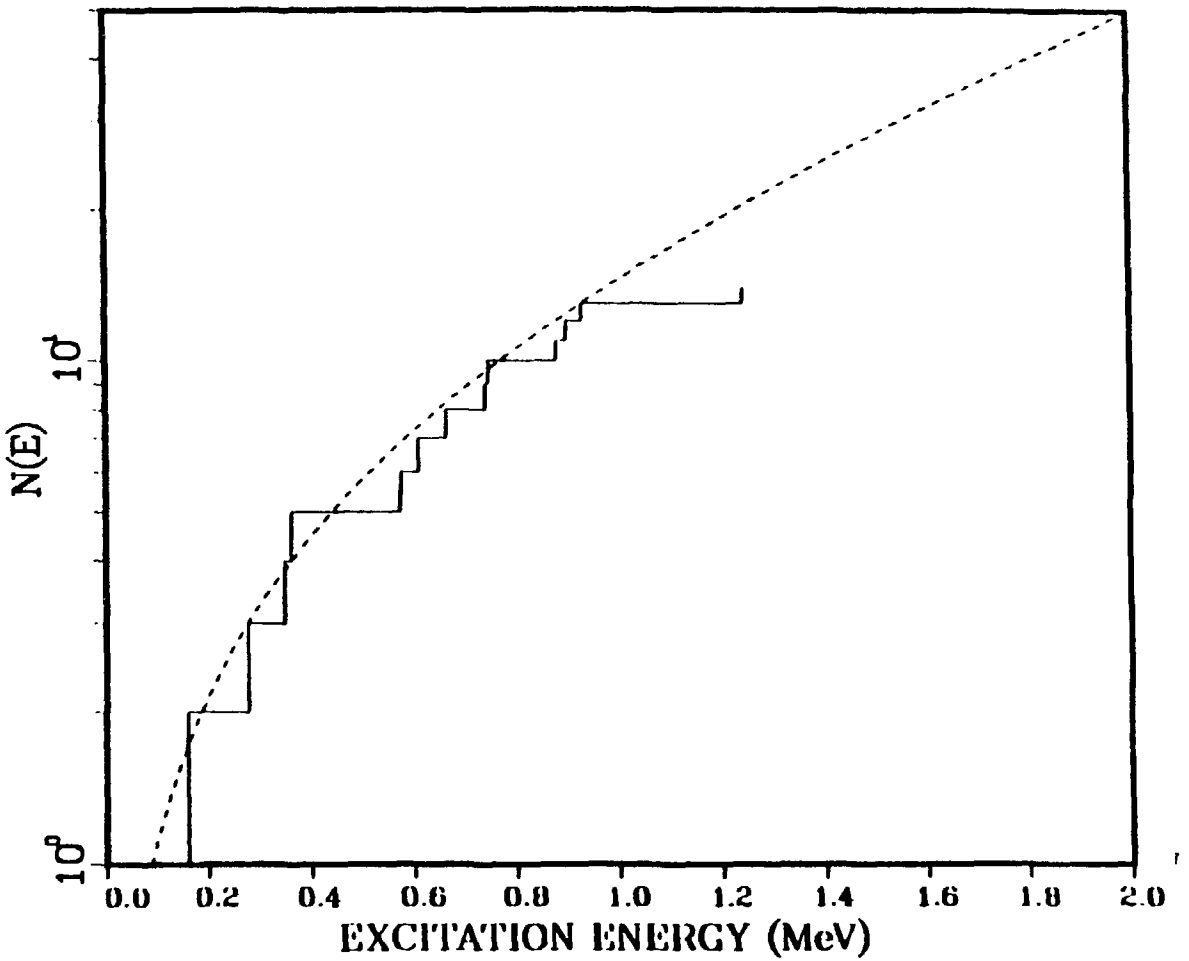

Figure 4.8 Experimental Levels and Level Fit of ^{64}Cu

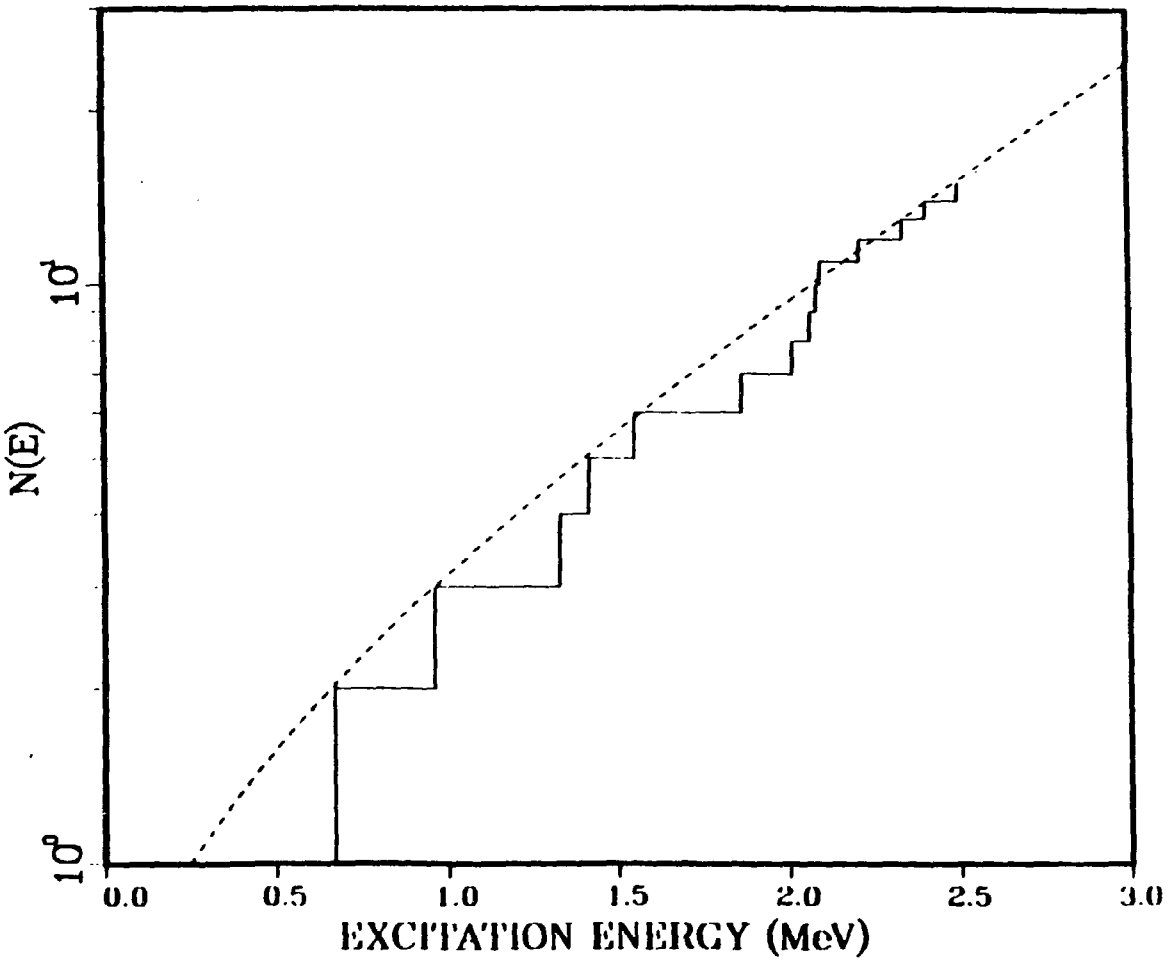

Figure 4.9 Experimental Levels and Level Fit of ^{63}Cu

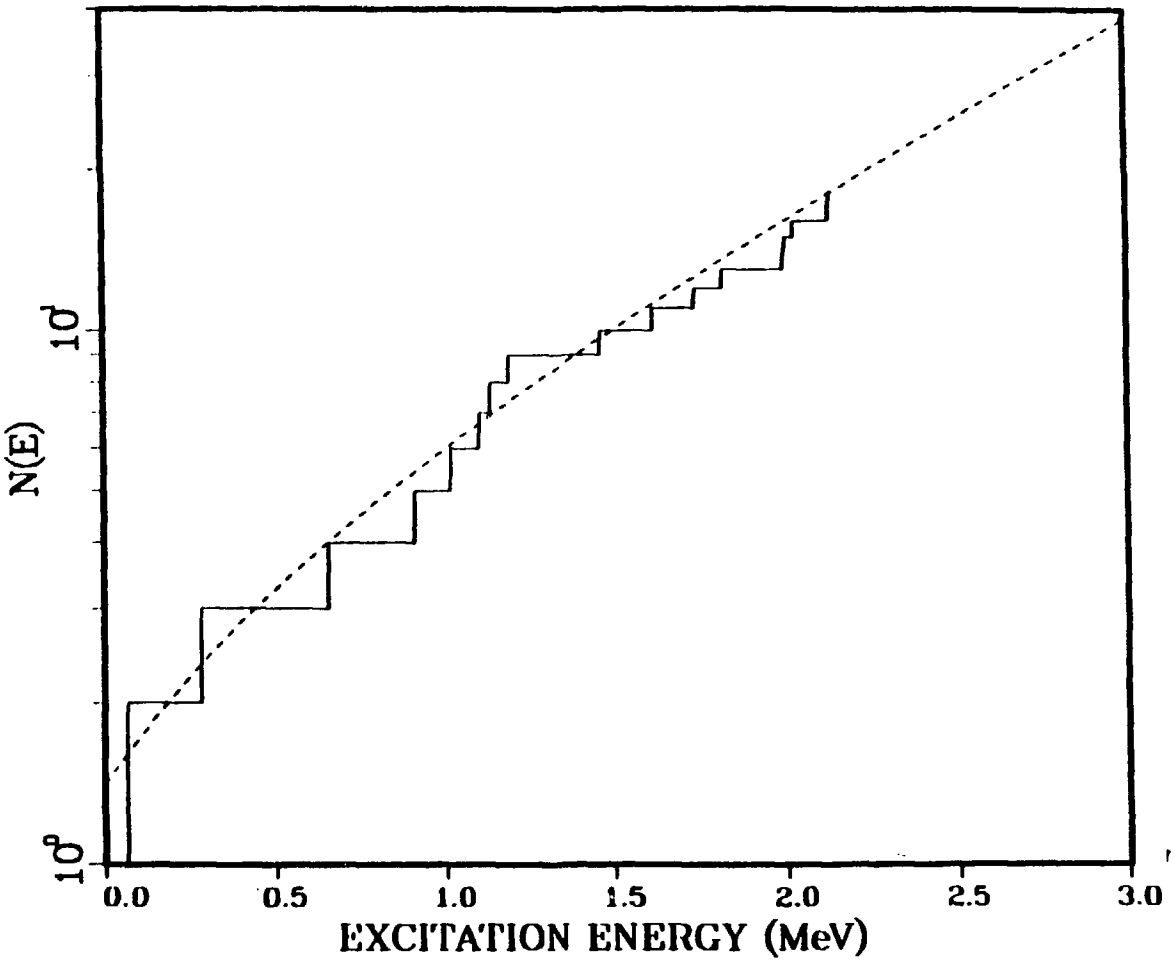

Figure 4.10 Experimental Levels and Level Fit of ^{61}Ni

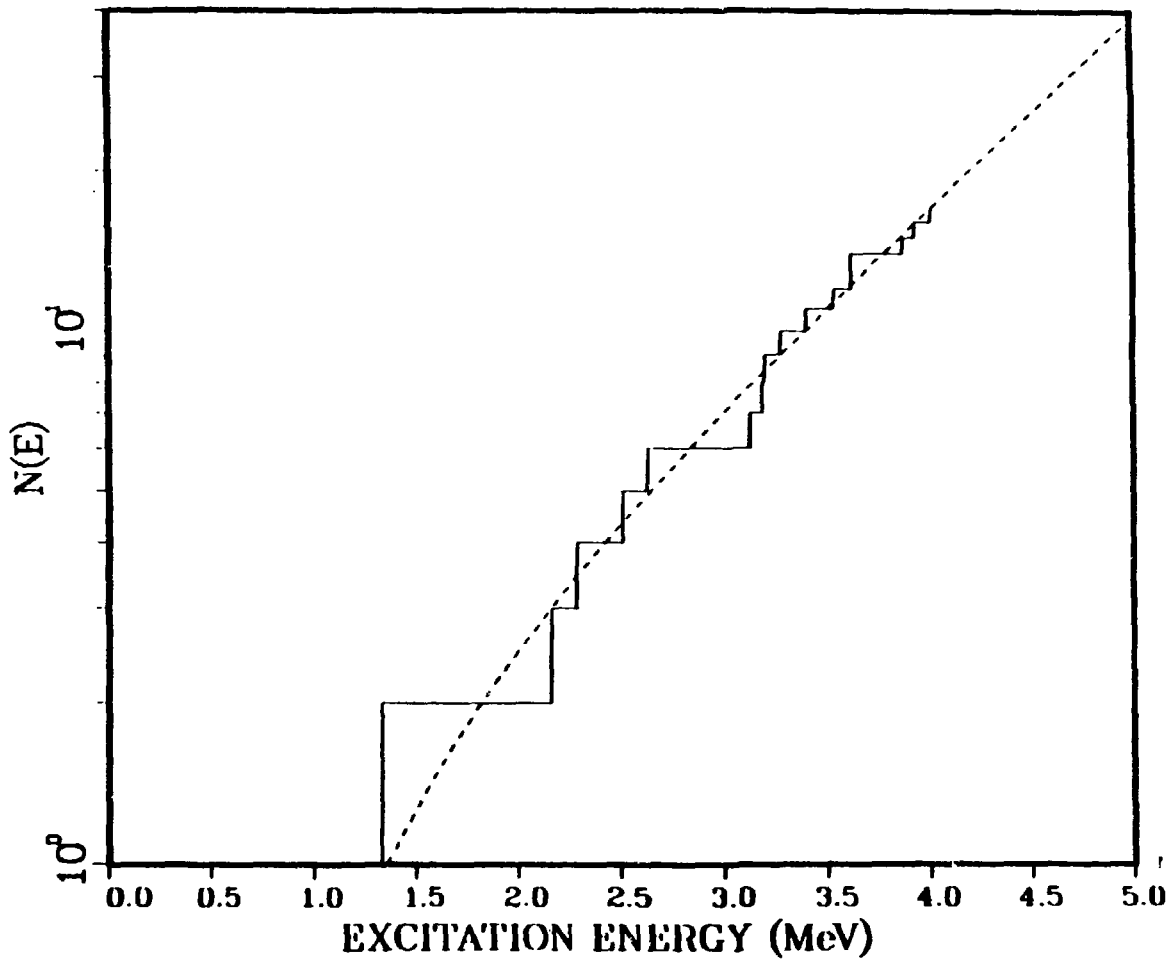

Figure 4.11 Experimental Levels and Level Fit of ^{60}Ni

J = total angular momentum,

Π = parity,

$\rho(e)$ = total level density for all states of the nucleus at excitation E.

The level density is assumed to be independent of parity, so that in the above equation:

$$F_{\Pi} = 1/2 \qquad (4.10)$$

The angular-momentum dependence is:

$$F_j(J,E) = [(2J + 1)/2\sigma^2]e^{[-(J+1/2)^2/2\sigma^2]} \qquad (4.11)$$

where σ is the spin cutoff parameter. The spin cutoff is given by the expression :

$$\sigma^2 = 0.146(aU)^{1/2}A^{2/3} \qquad (4.12)$$

where, A is the atomic mass (AMU) and a is the Fermi-gas level density parameter (MeV^{-1}) given by:

$$a = 9.17\ (MeV^{-1}) * 10^{-3}S_o + S_1 \qquad (4.13)$$

with, $S_o = S(n) + S(z)$ and $S_1 = 0.142\ (MeV^{-1})$, where S(n) and S(z) are the neutron and proton shell correction factors as tabulated by Gilbert and Cameron [17].

The first region is the one where experimental data exists as seen in Figure 4.2. In the second region, the temperature region, the equation for the energy dependence of the level density becomes:

$$\rho_T(E_x) = (1/T)e^{[(E_x-E_o)/T]} \qquad (4.14)$$

where, E_x is excitation energy of the residual nucleus, T is the characteristic nuclear temperature, and E_o is an adjustable parameter.
In the third region, defined as the Fermi gas region, the equation becomes:

$$\rho_{FG} = (\sqrt{\pi}/12)[e^{(2\sqrt{au})}/a^{1/4}U^{5/4}](1/2\sqrt{\pi}\,\sigma) \qquad (4.15)$$

Thus the matching of the temperature and level density functions is accomplished by requiring that:

$$\rho_T(E_m) = \rho_{FG}(E_m) \qquad (4.16)$$

$$\rho'(E_m) = \rho'_{FG}(E_m) \qquad (4.17)$$

$$\int_o^{E_c} \rho_T(E)dE = N_{exp}(E_c) \qquad (4.18)$$

where E_m is the matching energy for the temperature and Fermi gas regions, and N_{exp} is the number of discrete levels observed experimentally up to an excitation energy E_c.

4.5 Non-equilibrium Reactions

The compound nucleus has been modeled in a discrete statistical manner according to the Hauser-Feshbach theory. At very low energies where the wavelength of the neutron is large, compound nucleus processes dominate, and the neutron interacts with the nucleus as a whole. The opposite extreme occurs at higher energies, where the neutron interacts directly with small numbers of individual nucleons within the nucleus. These direct processes occur with characteristic times of 10^{-21} seconds. Because compound nucleus processes occur on a much longer time scale 10^{-16} seconds, one must also account for interactions at intermediate times. Therefore, two other models are introduced to account for these faster processes, namely, a direct reaction model and the preequilibrium model. The above processes are shown in Figure 4.12.

REACTION MODELS SCHEMATIC

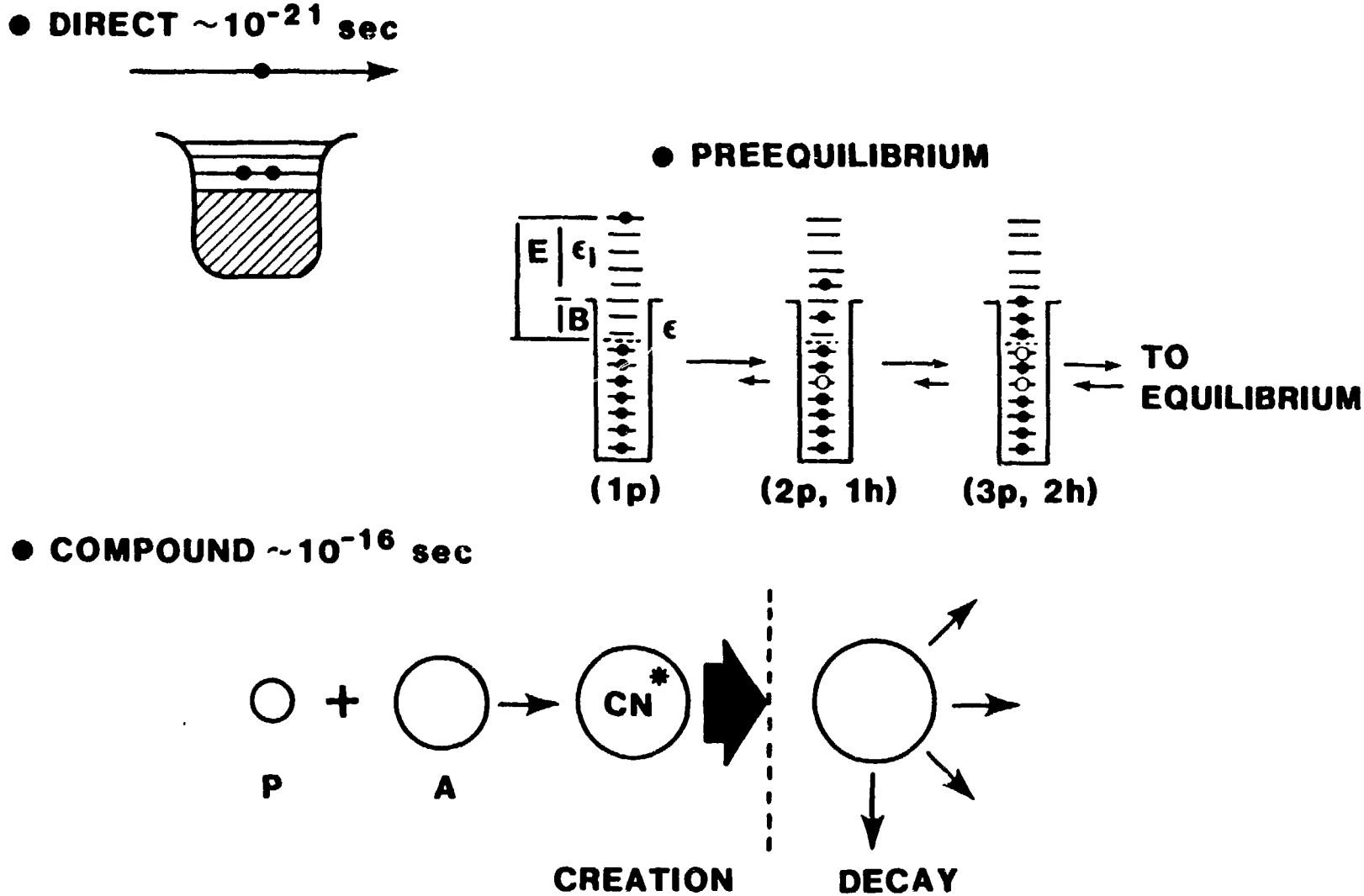

Figure 4.12 Schematic Illustration of Reaction Models

Direct reactions become important in the low MeV region, and preequilibrium reactions become important at 10 MeV. These are described in the following two sections.

4.5.1 Preequilibrium Model

The preequilibrium subroutine that is within the GNASH code is based on the exciton model of Kalbach [22]. As the name implies, one is trying to describe more accurately what is happening as the compound nucleus is formed, in a nonstatistical approach. The formation and decay of the average nuclear state proceeds through a series of two body interactions coupled with energy conservation. In this model, the nucleus is seen at varying "snapshots" in time according to the number of holes and particles at that time. The fraction of cross section that is described by the preequilibrium model is important in the overall cross section calculation. In this calculation, the parameters were adjusted such that a preequilibrium fraction of 0.25 occured at E_n = 14.8 MeV; that is, 25 percent of the neutron emissions proceeded through a preequilibrium mechanism. This value of the preequilibrium ratio has been found to reproduce measured neutron emission spectra in this mass region.

4.5.2 Direct Reaction Cross Section Model

Even with the Hauser-Feshbach statistical model and the pree-quilibrium model, the excitation of all the states produced are not adequately described. Therefore, the Distorted Wave Born Approximation was used for a more adequate description of direct reaction effects. The program DWUCK was applied along with the appropriate neutron optical model parameters to compute the relative direct cross sections [18]. These results were used in order to fine tune the GNASH cross section calculations. The absolute cross sections were calculated using the equation:

$$\sigma(\ell) = \text{beta}_{\ell}^{2} \ \sigma(\ell_{DWBA}) \qquad (4.19)$$

where ℓ is the neutron momentum transfer of the reaction and beta_{ℓ} is the deformation parameter obtained from proton inelastic scattering results. The beta values were taken from a paper by Johnson and Jones [23]. The quantity $\sigma_{DWBA}(\ell)$ resulted from the DWUCK calculations. The inclusion of direct reaction effects in the calculations increased the total inelastic cross section by 25 percent near 14.8 MeV, whereas the (n,p) and (n,2n) cross sections were decreased by 7 and 12 percent respectively.

4.6 The Optical Model and Parameter Determination for the Neutron Optical Model

Since the discovery of the neutron in 1932, people have expanded and developed the field of neutron physics with fervor. This advance-ment has occurred both through experimentally advancing neutron physics,

and through the development of theoretical models that account for the experimental phenomena. Since a phenomena can be described as the results of the action of the different forces upon matter, sometimes theoretical modeling aids in the futuristic projections of what has not or cannot be experimentally observed. This becomes especially applicable in the previously discussed Hauser-Feshbach statistical model. One needs an approach that combines insight and theory along with the experimental results. Therefore, the optical model gives the appropriate parameters through a combination of experimental data and theoretical assumptions to produce the input needed for the GNASH code.

In order to run the GNASH code, a suitable optical model and its parameters must be determined. In fact good results depend strongly upon this accurate optical model. It should be noted that the purpose of the optical model is to provide transmission coefficients consistent with a wide range of of neutron cross section measurements. Even though the Hauser-Feshbach statistical model aids in the delineation of the problem, it is entirely dependent on the transmission coefficients used in the calculations. "The statistical nature of the compound nucleus theory implies that its predictions are at best averages, and do not take into account the differences between specific nuclei. It is not surprising, therefore, that a more detailed model is needed for the description of nuclear reactions" [24].

The optical model describes the effect of the nucleus on the incident particle by a potential well V_R, but allows for the possibility of compound nucleus formation by adding to the potential a negative imaginary part, -W. This part produces an absorption of the incident particle by the nucleus, and this absorption represents the formation of

the compound nucleus. With the optical model, compound nucleus formation does not occur immediately. Even if the incident particle has entered the nucleus, it is removed from its free particle state only with some delay and with a certain probability. If V_R and W are reasonably constant over the nucleus, it is possible to define a coalescence coefficient which is the probability per unit length for the incident particle in nuclear matter to form the compound nucleus.

In the optical model, the nucleus is not "black" to the wave representing the incident particle; instead it acts like a gray sphere, partly absorbing and partly refracting the incoming wave. There is an analogy with physical optics in that the nucleus acts like a spherical region with a given refractive index (attractive well potential well) and opacity.

To determine the optical model parameters, a fitting code (SCATOP) was used [25]. For the purpose of this work, it was determined to approach the problem simply using a spherical optical model code. First, it should be noted that the code allows for the variation of incident particle types: i.e., incident neutrons, protons, deuterons,etc., and initial values for the optical potential must be provided before actually fitting the data.

The following optical form was assumed for the neutron optical potential:

$$U = -V_R f(r, a_R, R_R) + 4ia_D W_D \, d/dr \, f(r, a_D, R_D) - i W_V f(r, a_V, R_V) + 2\lambda_\pi^2 V_{SO} \vec{l} \cdot \vec{s} \, (1/r) \, d/dr \, f(r, a_{SO}, R_{SO}) \qquad (4.20)$$

with Saxon-Woods form factors,

$$f(r, a_i, R_i) = [1 + e^{(r-R_i)/a_i}]^{-1} \qquad (4.21)$$

where, R_i is equal to $r_i A^{1/3}$.

The four terms in the potential expression represent a real central potential (V_R), a surface derivative imaginary (absorptive) potential (W_D), a volume imaginary term (W_V), and a spin-orbit term (V_{SO}). The quantity λ_π is the pion Compton wavelength (from meson field theory of nuclear forces), and A is the atomic mass of the target nucleus.

The quantities r_i and a_i specify a radius and a diffusivity for the form factor associated with each term. The following forms were assumed for the potential depths:

$$V_R = V_o + \alpha E \tag{4.22}$$

$$W_D = W_{do} + \beta E \tag{4.23}$$

$$W_V = W_{vo} + \delta E \tag{4.24}$$

$$V_{SO} = \text{constant} \tag{4.25}$$

Experimental elastic angular cross sections, total cross sections and low energy average resonance data were fit. Initially, no correction was made for the fact that the code calculates shape elastic cross sections only, whereas the measurements include shape and compound elastic cross sections. This assumption is reasonable, however, because the fitting does not include data from low energies, where compound elastic effects are largest. Also, initially, the potential depths of V_o, W_{vo} and W_{do} along with V_{SO} were taken from the parameters developed by Arthur for nickel [26]. Then further development of the parameters was completed as the calculations were refined.

The low energy resonance parameters that were fit were the neutron s- and p- wave strength functions (S_o and S_1) and the potential scattering radius (r'). Values for these quantities and their uncertainties were obtained from "Neutron Cross Sections", by Mughabghab [27]. Also included in the fit were six neutron elastic scattering angular distributions at ten different energies between 3.2 and 14 MeV. Finally, neutron total cross sections up to 20 MeV were included to insure accurate reaction and total cross sections. All fitting was accomplished by minimizing the chi-squared values given by:

$$x^2 = \sum^{N} (\text{Exp.} - \text{Obs.})^2 \ /(N - 1) \qquad (4.26)$$

where N is the number of experimental values in the fit.

For the first iteration of the program, W_{DO} the imaginary surface well depth together with the diffuseness a_D was varied until a minimum x^2 value was achieved. After that, the energy dependence β followed by the real well depth V_R was varied to achieve more accurate results. Finally, the radii r_R and r_D were optimized. Therefore, the procedure that was followed was initially to vary the imaginary parameters and then to vary the real parameters. In the final interations, it was determined that the energy dependence in W_D was not required to make a significant change in the fitting.

Neither the volume nor the spin orbit potentials were important to determine cross sections below 20 MeV, so the values of Harper et al. for Ni were used [28]. The set of parameters obtained from the fit were used in preliminary GNASH calculations to obtain estimates of the compound elastic cross section at each energy where elastic angular distribution were fit. A complete second iteration was then made,

repeating the above steps, after correcting the angular distributions for compound elastic contributions.

Figure 4.13 shows the calculated total cross sections between neutron energies from 1.0-20.0 MeV compared to the experimental data of Foster [29]. The elastic angular distributions in Figures 4.14-4.16 depict the comparison of the theoretically derived values to the experimentally measured values for incident neutron energies of 3.4, 8.0 and 14.0 MeV. Results for the optical model neutron potential are shown in Table 4.1. These parameters give the best chi-squared results and they also reproduce the S_o, S_1, and the r' values as seen in Table 4.2.

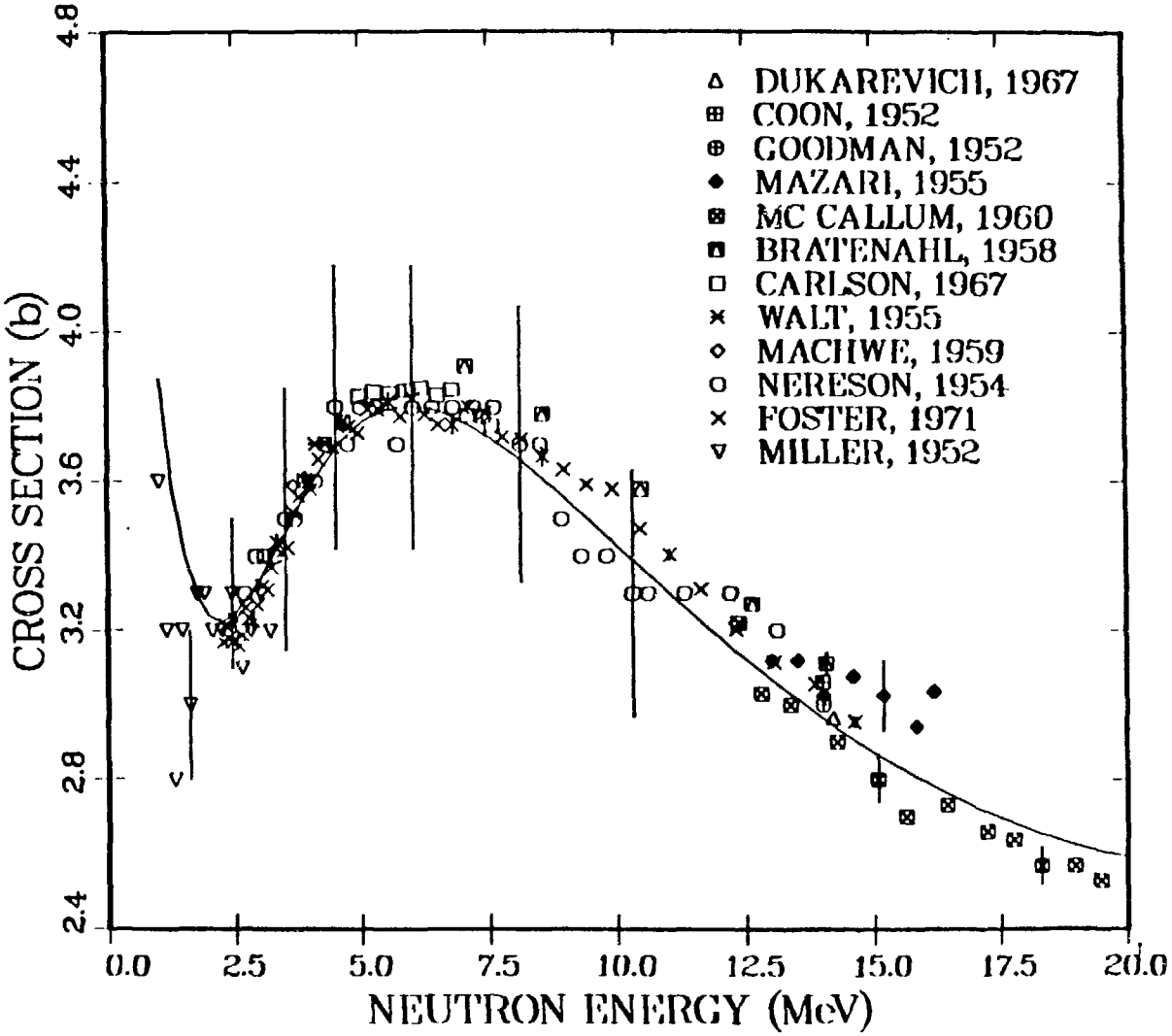

Figure 4.13 Comparison of Theoretical and Experimental Values of n + Zn Total Cross Sections from 0.0 – 20.0 MeV

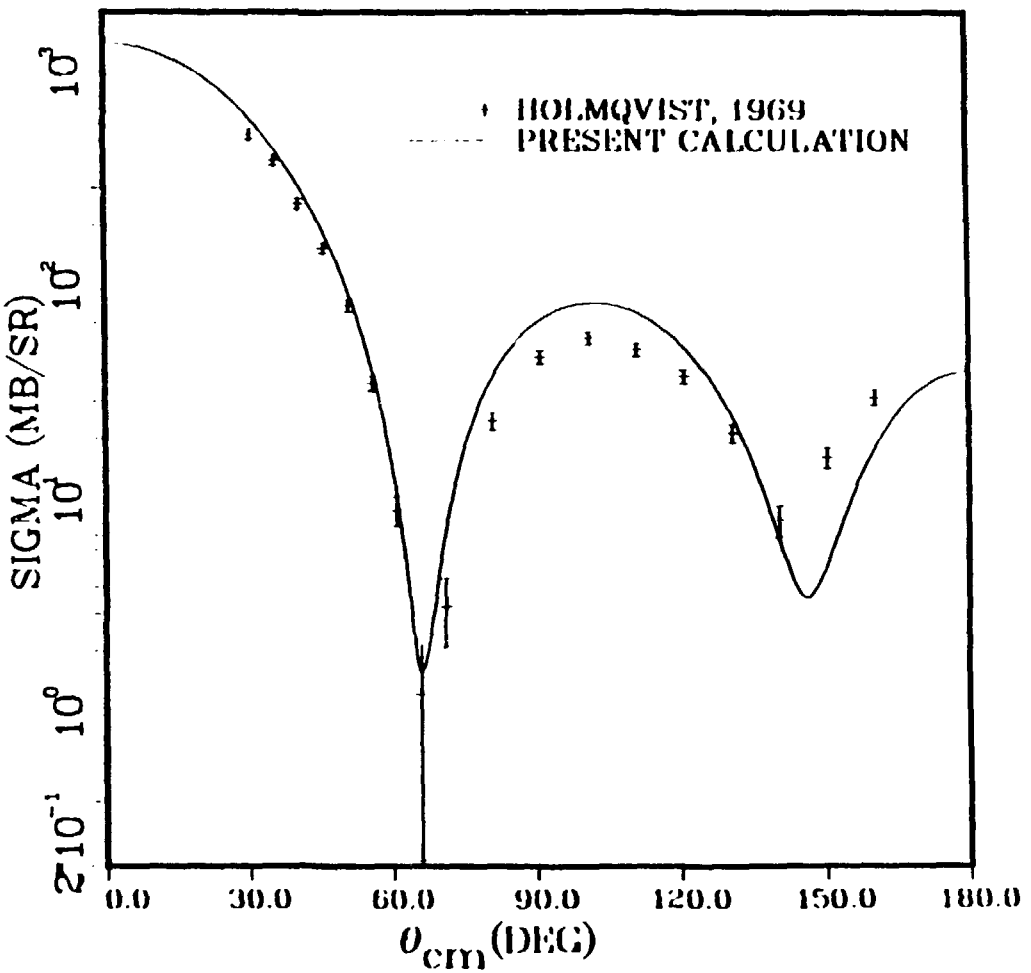

Figure 4.14 Comparison of Theoretical and Experimental Values Obtained for ^{64}Zn + n Elastic with E_N = 3.44 MeV

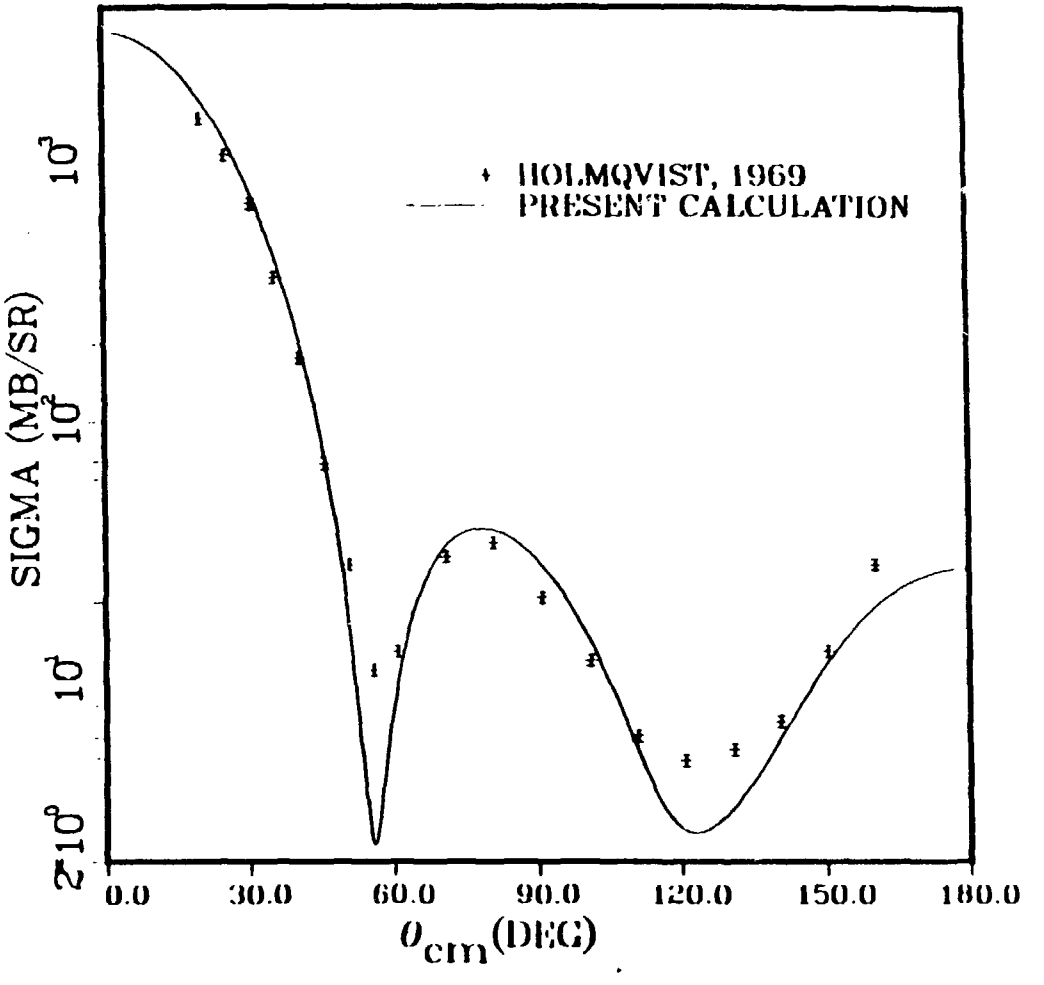

Figure 4.15 Comparison of Theoretical and Experimental Values Obtained for ^{64}Zn plus (+) n Elastic with E_N=8.05 MeV

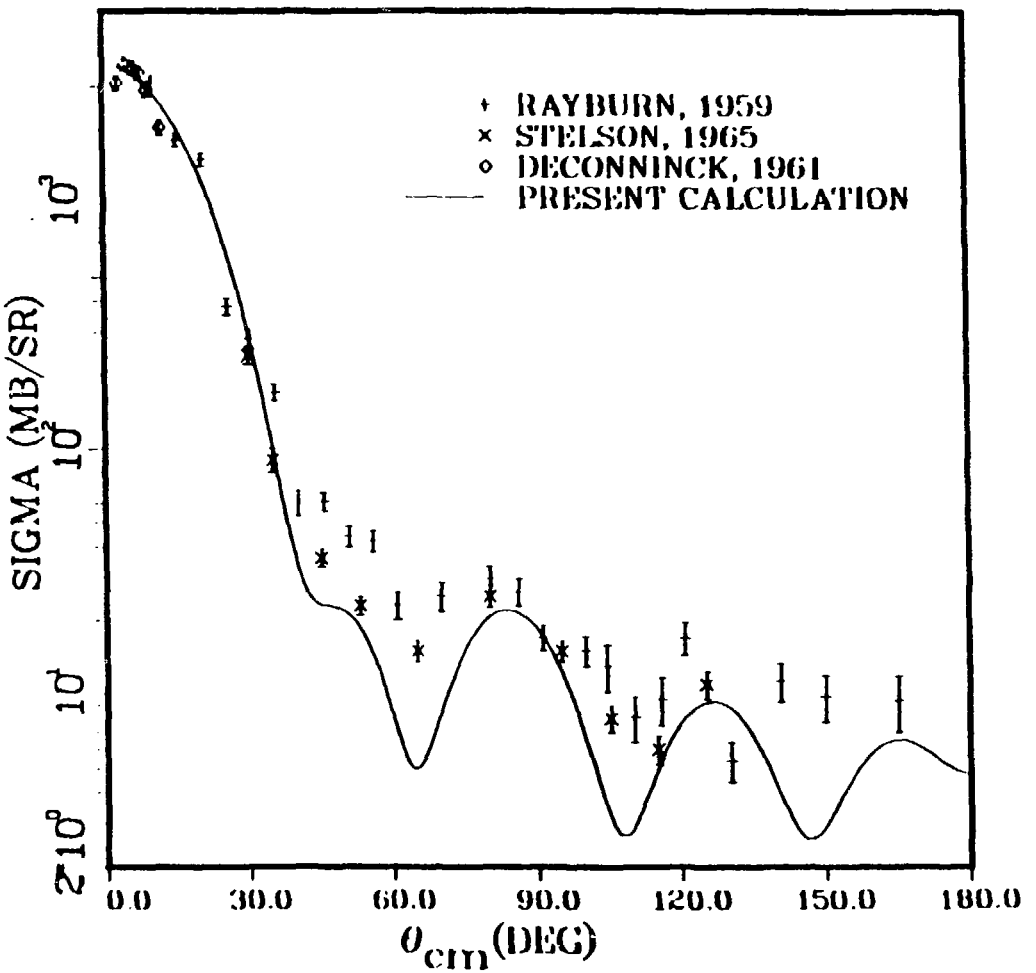

Figure 4.16 Comparison of Theoretical and Experimental Values Obtained for ^{64}Zn + n Elastic with $E_N = 14.0$ MeV

Table 4.1

Optical Model Potentials

Potential (MeV)	r_i (fm)	a_i (fm)
V_R = 48.11 - 0.376E	1.295	0.58
W_D = 8.045	1.295	0.48
W_V = -0.094 + 0.197E	1.295	0.58
V_{SO} = 6.2	1.12	0.48

Table 4.2

Average Resonance Parameters

	$S_0(10^{-4})$	$S_1(10^{-4})$	R' (fm)
Experiment	1.70 ± .16	0.60 ± .04	7.0 ± .7
Optical Model	1.97	1.05	7.3

4.7 The Optical Model and Parameter Determination for the Proton and Alpha Optical Model

Similar to the neutron case, a spherical optical model was used for alphas and protons. The proton optical model potential was taken from the work of Perey [8]. Variations of this potential by Arthur and Young were also tried, but the simpler Perey potential gave essentially equivalent results below 20 MeV. The alpha particle parameters were also taken from the parameters derived for iron by Arthur and Young [8].

In the case of protons, the parameters were checked by GNASH calculations of (p,n) cross sections. This was done for ^{65}Cu (p,n)^{65}Zn and for ^{63}Cu (p,n)^{63}Zn interactions. A complete discussion of GNASH calculations is given in Section 4.2.

The results for the (p,n) calculations can be seen in Figures 4.17-4.18, and the overall agreement between the calculated (p,n) cross sections and measured values is very good. In the case of ^{63}Cu, the lower energy region was in reasonable agreement for both sets of experimental data. Between 6.0 and 10.0 MeV, the agreement is not as good because of possible inaccuracies in the experimental values. Between 10.0 and 20.0 MeV, once again the agreement is excellent. This shows that the optical model values chosen were in general very good.

As for the ^{65}Cu check between the experimental and theoretical values, overall agreement was much more consistent than the ^{63}Cu values, especially below 12.0 MeV. As can be seen in Figure 4.18, in general the GNASH calculations were within the determined experimental error below 12.0 MeV. Even at higher energies the calculations follow the overall trend of the data and the proton potential was judged to be

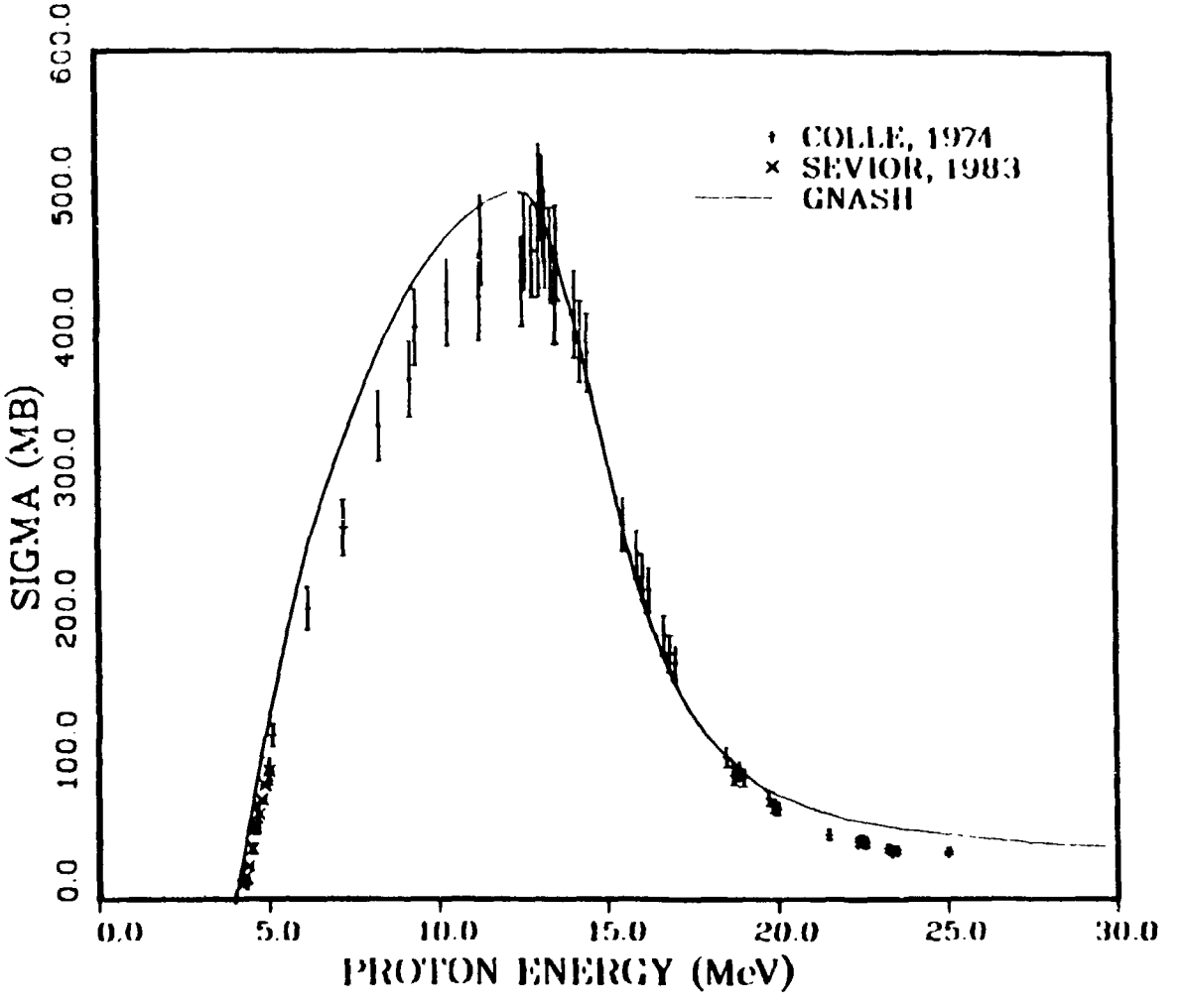

Figure 4.17 Comparison of Experimental and Theoretical Values Obtained for the ^{63}Cu (p, n) ^{63}Zn Cross Sections from 0.0 – 30.0 MeV

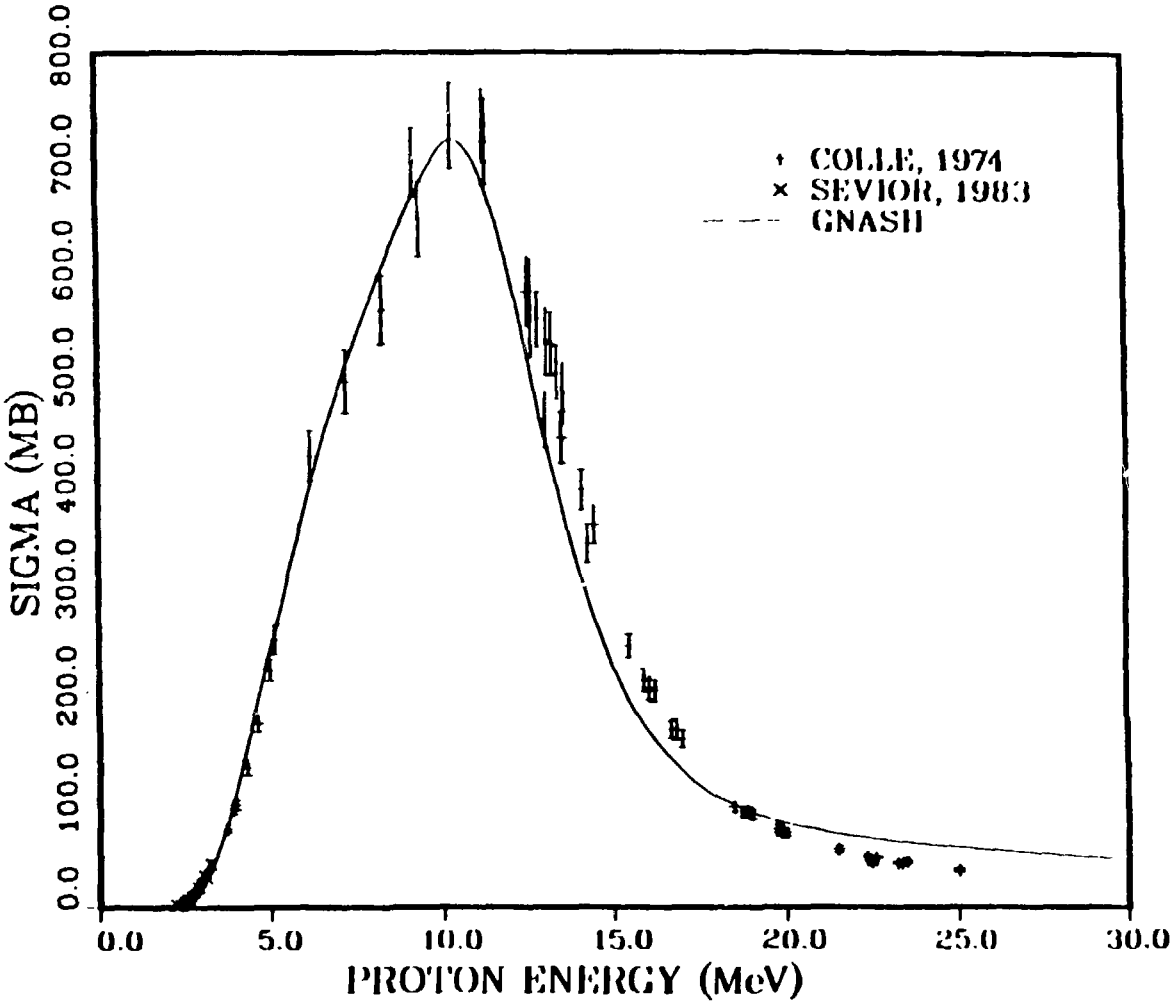

Figure 4.18 Comparison of Experimental and Theoretical Values Obtained for the ^{65}Cu (p, n) ^{65}Zn Cross Sections from 0.0 - 30.0 MeV

adequate for the present calculations. The final proton optical model parameters for zinc are give in Table 4.3.

Table 4.3

Proton Optical Model Parameters

Potential (MeV)	r_i (fm)	a_i (fm)	
V_R = 58.73 - 0.55E	1.25	0.65	
W_D = 13.5	1.25	0.47	E<12

The optical model parameters for alpha particles were taken from the work that was done for iron. These parameters are shown in Table 4.4

Table 4.4

Alpha Optical Model Parameters

Potential (MeV)	r_i (fm)	a_i (fm)
V_R = 193.0 - 0.15E	1.37	0.56
W_V = 21.0 + 0.25E	1.37	0.56

In summary, the optical model parameters that achieved the best results with the GNASH code were the Young-Rutherford parameters obtained here for neutrons, the Perey parameters for the protons, and the Arthur-Young parameters for the alphas.

4.8 Gamma Ray Transmission Coefficients

Just as the optical model produced important and accurate transmission coefficients for neutrons, protons, and alpha particles, so too must the gamma ray transmission coefficients be determined as input for the GNASH code, because the code tracks gamma ray emission as one of the decay processes. The gamma ray strength functions were calculated from equations based on a giant-dipole resonance model [30]. The calculated strength function shapes were renormalized to agree with values of $2\Pi \langle\Gamma_{\gamma o}\rangle/\langle D_o\rangle$ inferred from experimental determinations of $\langle\Gamma_{\gamma o}\rangle$, the average radiative capture width for s-wave resonances, and $\langle D_o\rangle$, the average level spacing observed with s-wave reactions. Thus, the gamma-ray transmission coefficients were obtained from the renormalized strength functions. See the above reference for a more complete description of the technique.

CHAPTER FIVE

RESULTS AND CONCLUSIONS

5.1 Introduction

Accurate measurements of the ^{64}Zn (n,2n)^{63}Zn and ^{64}Zn (n,p)^{64}Cu cross sections for use in the fusion community have been the main goals of the present research. Even though the primary request was for use within the fusion reactor program, the results from this work will also be used in fission reactor applications.

These experimental measurements were compared with the same cross sections calculated by using the GNASH code at Los Alamos National Laboratory. The theoretical calculations provide an additional level of confidence to the measurements that did not exist previously. In addition, the GNASH code was used to predict these cross sections at energies ranging from 0.10 to 20.0 MeV, which were then compared with data taken from the National Nuclear Data Center at Brookhaven National Laboratory [19].

5.2 Analysis of Experimental Results

The new experiments were needed to achieve highly controlled and accurate data to use as an independent reference. The previous measurements of these cross sections, especially the ^{64}Zn (n,p) ^{64}Cu cross sections were deficient in many respects, as will be shown later in a selection of (n,p) and (n,2n) previous measurements. The errors associated with these measurements include noisy electronics, lack of a

good reference, an unstable detection system, and significant neutron flux variations. In the present cross section measurements, most of these errors have been reduced or eliminated.

As in any measurement, there is a certain amount of error. The sources of error in the present cross section measurements are divided into two categories: systematic and random or run dependent errors. Systematic errors include: a) errors associated with the decay scheme determination, b) the cross section used as a reference or standard, c) sample weight, and d) detector stability and calibration. Run dependent errors include: e) statistics, f) background, g) geometry, h) flux variation, i) change in neutron energy from run to run.

These sources of error are consistent with those identified by Ghanbari and Robertson for the cross section analysis of ^{63}Cu (n,2n) ^{62}Cu and ^{65}Cu (n,2n) ^{64}Cu which were the standards for the present experiment [7].

The systematic error in the present measurements are given in Table 5.1. In the systematic error analysis, decay schemes play a vital role. The half-life is used to determine the decay constant which enters into the saturated activity determination as shown in Chapter Three. The errors associated with ^{64}Cu (12.701 $\pm$ 0.002 hours) and ^{63}Zn (38.4 $\pm$ 0.2 minutes) half-lives are less than 1 percent. In concert the branching ratios are also used to determine the saturated activity. They are both quite different. The ^{64}Cu branching ratio (93 percent) was remeasured recently to give a very accurate percentage of beta-plus emission. The ^{63}Zn branching ratio (97 percent) has an uncertainty that is substantially larger than that for ^{64}Cu, as seen in Table 5.1.

The reference foils that were used to determine the cross sections have an error that was important to the analysis of the measurements. In fact, this is the most important single source of uncertainty. Thus for the ^{63}Cu (n,2n) ^{62}Cu cross section a standard value of 549 ± 11 millibarns was used, and for the ^{65}Cu (n,2n) ^{64}Cu cross section the value 968 ± 20 millibarns was used. Each of the above reference cross sections has an error that is approximately 2 percent, reported on the one sigma level.

Table 5.1

Systematic Errors Associated with Measurements

Systematic Errors	^{64}Zn (n,2n)^{63}Zn %	^{64}Zn (n,p)^{64}Cu %
Branching Ratio	± 1	± 0.1
Half-life	± 0.787	± 0.153
Sample Weight	± 0.001	± 0.001
Standard Cross Section	[^{62}Cu] ± 2	[^{64}Cu] ± 2
Detector Calibration	± 0.05	± 0.05

The random errors associated with the ^{64}Zn $(n,2n)^{63}Zn$ and ^{64}Zn $(n,p)^{64}Cu$ measurements are given in Tables 5.2 and 5.3 along with the cross section values determined from each individual measurement. Statistical errors were typically 0.2 percent. The background contribution to the error analysis was negligible. Geometry or the position of the foil was not a factor in the error determination for the measurements, because the two foils were placed in the same position for each run. Next, the flux variation as measured by the flux monitor was at the worst 1.0 percent while the average variation for the flux deviation was 0.5 percent. Since the flux is the same for the reference and sample foils, the effects cancel and the error associated with it is negligible. The gamma spectra emitted was analyzed on a multichannel analyzer to make sure there was no other contributing gamma radiation. Also, beta particle contributions were negligible because the foils were placed between two pieces of teflon, to stop any foreign beta contribution to the count rate.

Table 5.2

Random Errors Associated with the ^{64}Zn (n,2n) ^{63}Zn Measurement

Data Set	Cross Section (mb)	Stats. (%)	Bkgd. (%)	Flux (%)
Ap1786	202	0.17	0	0.55
Ja1286	200	0.20	0	0.65
Ja0786	198	0.16	0	0.70
Ja1986	199	0.10	0	0.50
Se0186	195	0.19	0	0.67
Se1286	202	0.27	0	0.71
Mean Value	199 ± 6			

Table 5.3

Random Errors Associated with the ^{64}Zn (n,p) ^{64}Cu Measurements

Data Set	Cross Section (mb)	Stats (%)	Bkgd. (%)	Flux. (%)
Ja1686	177	0.20	0	1.0
Fe1186	177	0.15	0	0.67
Ma0386	175	0.12	0	0.50
Mean Value	176 ± 4.5			

Each of the individual measurements in Tables 5.2 and 5.3 consists of an average of at least three different sets of disintegrations/second taken over the same time period (100 seconds), also statistically valid within the characteristic half-life. At the bottom of each table is given the average cross section from all the measurements, together with the total uncertainty on the one sigma level from all sources (random and systematic). The (n,2n) data was taken within the characteristic half-life for ^{63}Zn which is 38.1 minutes, and the averaged value is 199 ± 6 millibarns. In the case of the ^{64}Zn (n,p) ^{64}Cu data, ten sets of

counts were chosen within the half-life (12.71 hours) and averaged for the value presented of 176 ± 4.5 millibarns. The equations that were used to calculate the deviation in the measurements were taken from Knoll [10].

The usual criteria are to have six separate sets of data to provide statistical accuracy and to verify reproducibility. The three measurements of the ^{64}Zn (n,p) ^{64}Cu however, are quite consistent. In the case of the ^{64}Zn (n,2n) ^{63}Zn there is good agreement in the six sets of values and enough data for high statistical accuracy. Both sets of measurements represent a good poisson distribution and the ^{64}Zn (n,p)^{64}Cu results are consistent with the poisson distribution.

5.3 Analysis of Theoretical Results

As described in Chapter Four, the theoretical cross section calculations were based on Hauser-Feshbach statistical, preequilibrium, and direct reaction models. Alphas, neutrons, protons and gamma-rays were the emissions chosen for the particle decay chain in the GNASH code, while neutrons and protons were the incident particles. SCATOP was used to determine the optical model parameters presented in Chapter Four [25]. Transmission coefficients were calculated from these parameters. The transmission coefficients determined for this research (especially the neutron transmission coefficients) were very accurate. They produced good reaction cross sections and accurately described particle emission over a wide range of emission energies.

The quantities calculated by GNASH include cross sections and emission spectra for (n,γ), (n,n'), (n,p), (n,α), (n,2n), (n,np) and (n,nα) reactions from ^{64}Zn.

5.4 Comparison of Experimental and Theoretical Results

The measured and calculated ^{64}Zn (n,2n)^{63}Zn cross sections at 14.8 MeV are in excellent agreement (1 percent). As seen in Figure 5.1 and 5.2, this agreement is the best of all the measured values. This is due primarily to having reliable neutron optical model parameters; that is, the (n,2n) calculation is somewhat insensitive to the proton parameters. Over the whole energy range, Paulsen's results agree with the theoretical calculations [31]. Other authors such as Bormann agree with the (n,2n) theoretical calculations around the 12.0 - 15.0 MeV energy range and then diverge rapidly at higher energies [32]. This is seen clearly in Figure 5.2. Between 12.0 and 20.0 MeV, Weigold and Rao's results also agree with the GNASH calculations for the (n,2n) measurement [33,34].

As shown in Figures 5.3, 5.4 and 5.5 the measured and theoretical cross sections for the ^{64}Zn (n,p)^{64}Cu reaction are also in good agreement (4 percent). This difference is larger than the (n,2n) case possibly due to the optical model for charged particles. That is, it is possible that the competition from protons is slightly underpredicted at some energies. In the lower energy region, the agreement of calculated and measured results is very good. Between 5.0 and 12.5 MeV, there is considerable discrepancy among the experimental data. This is shown in

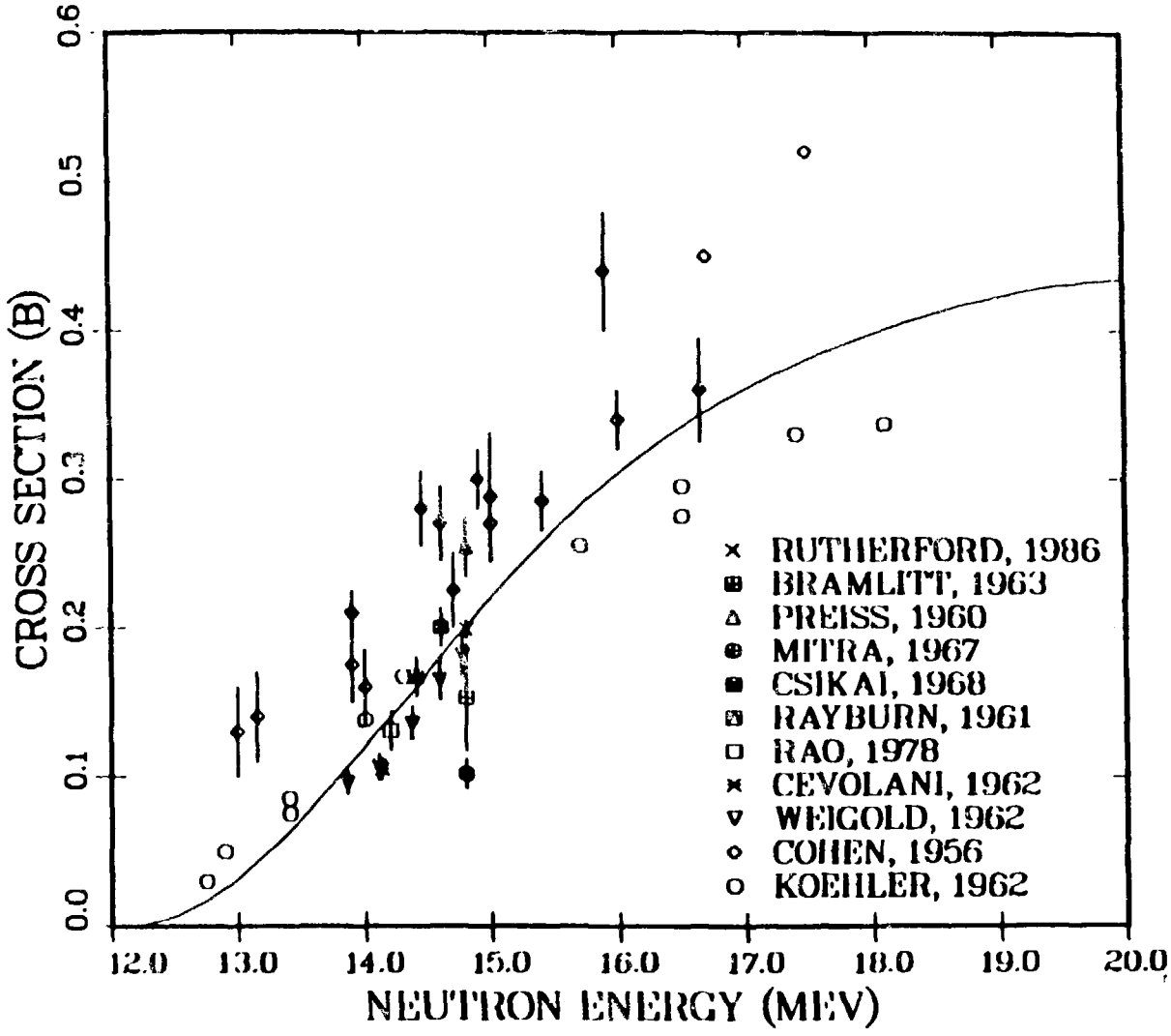

Figure 5.1 Comparison of Experimental and Theoretical Values of ^{64}Zn (n, 2n) ^{63}Zn Cross Sections from 12.0 – 20.0 MeV

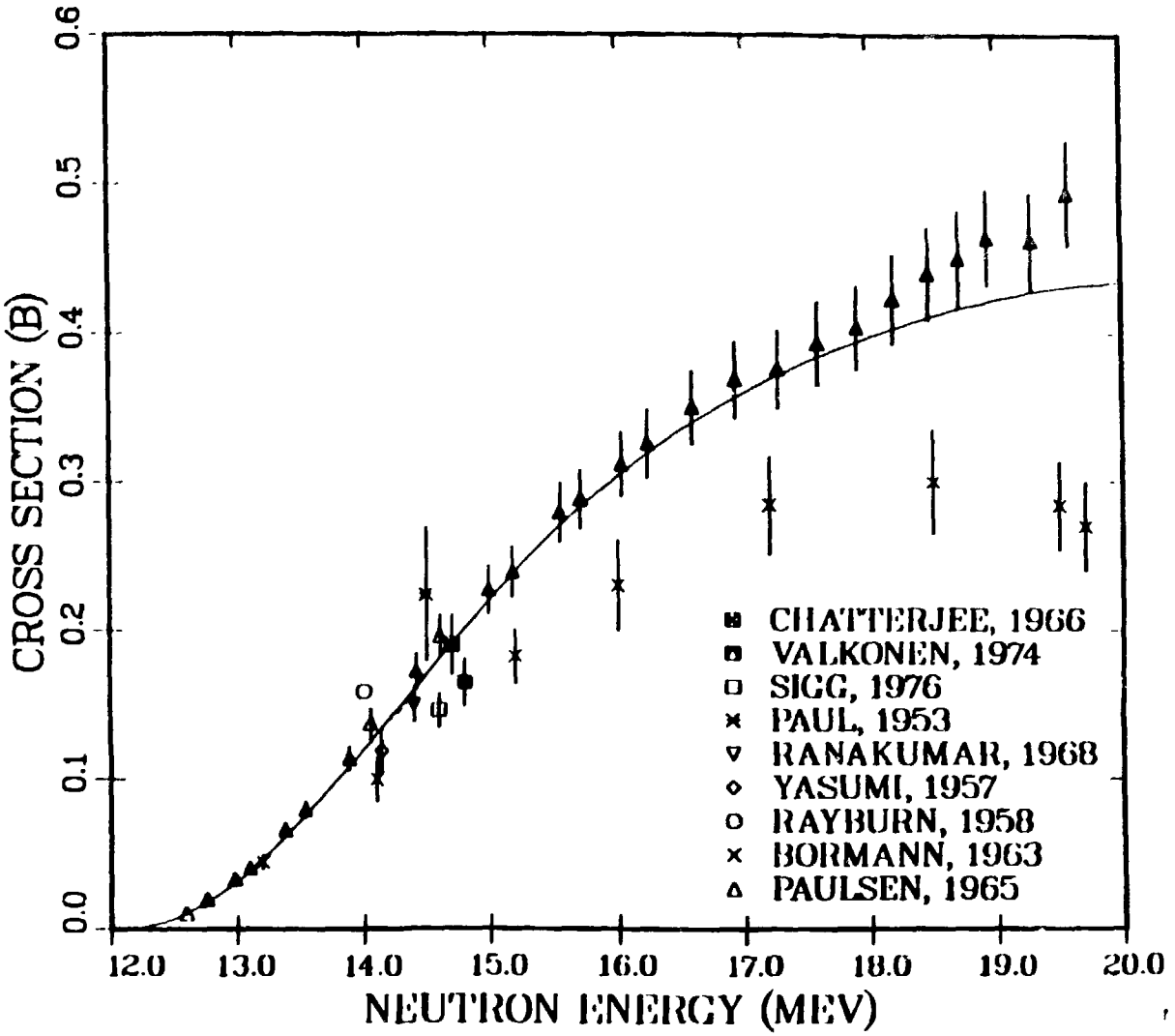

Figure 5.2 Comparison of Experimental and Theoretical Values of ^{64}Zn (n, 2n) ^{63}Zn Cross Sections from 12.0 - 20.0 MeV

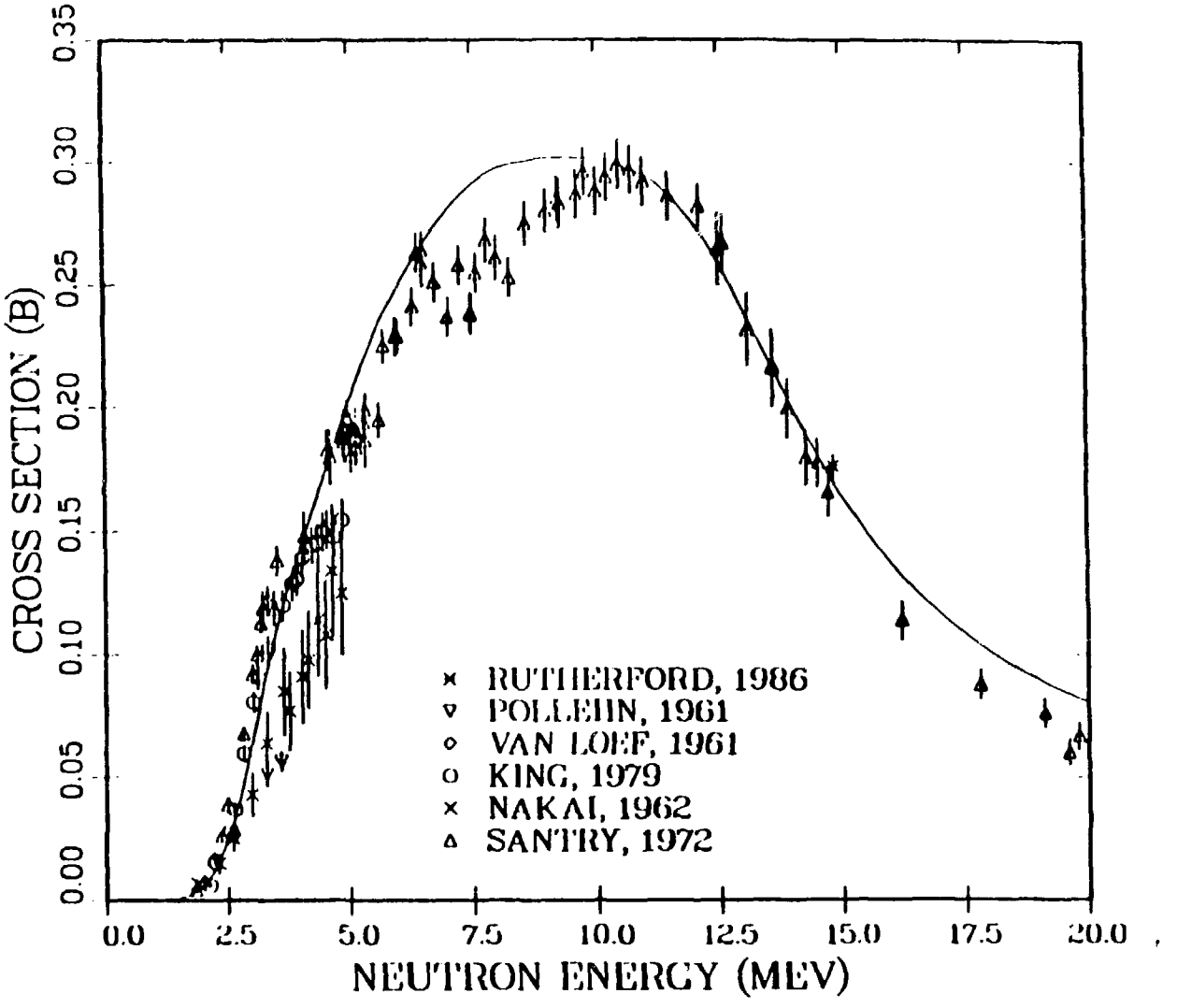

Figure 5.3 Comparison of Experimental and Theoretical Values of ^{64}Zn (n, p) ^{64}Cu Cross Sections from 0.0 - 20.0 MeV

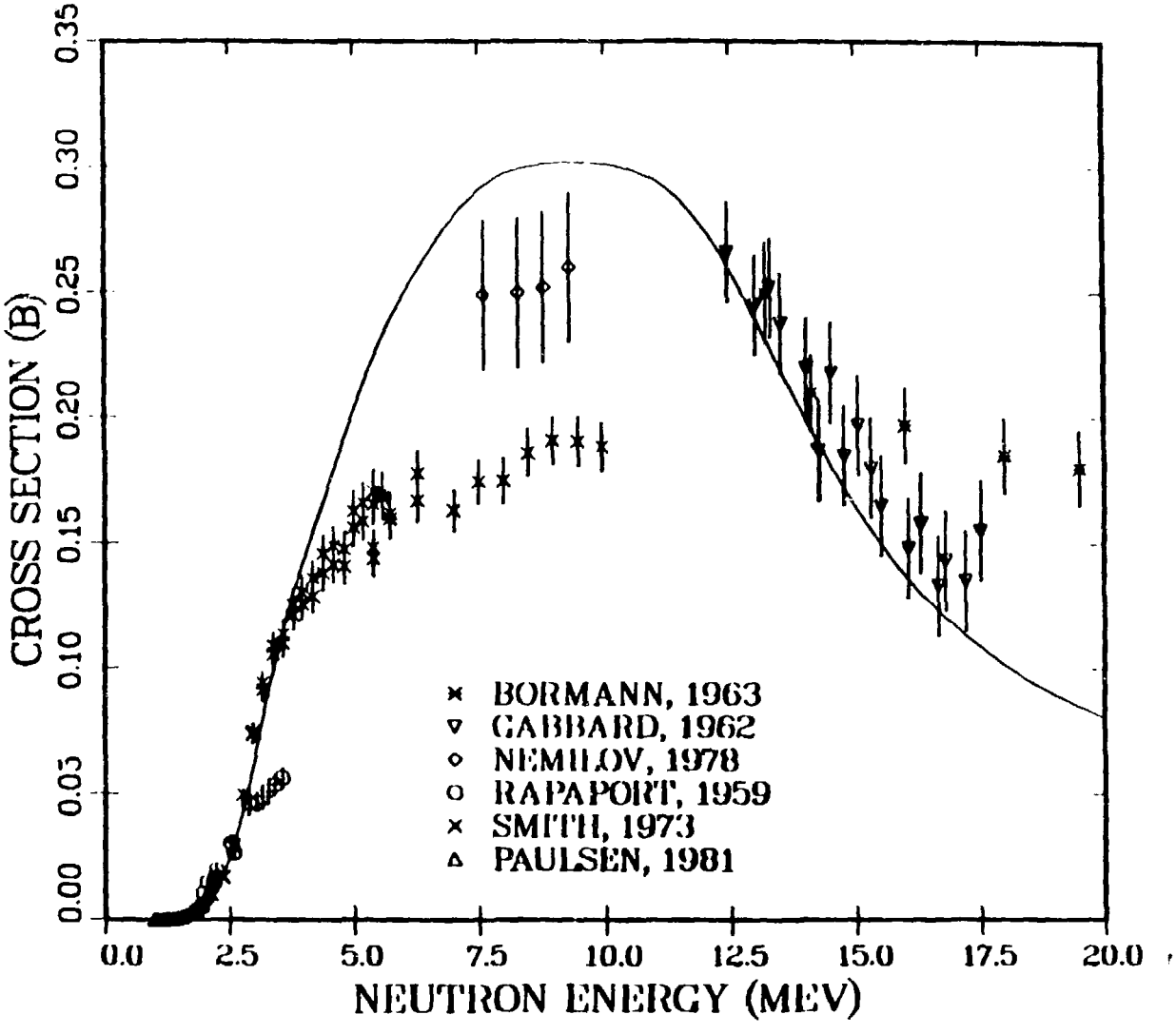

Figure 5.4 Comparison of Experimental and Theoretical Values Obtained for ^{64}Zn (n, p) ^{64}Cu Cross Sections from 0.0 – 20.0 MeV

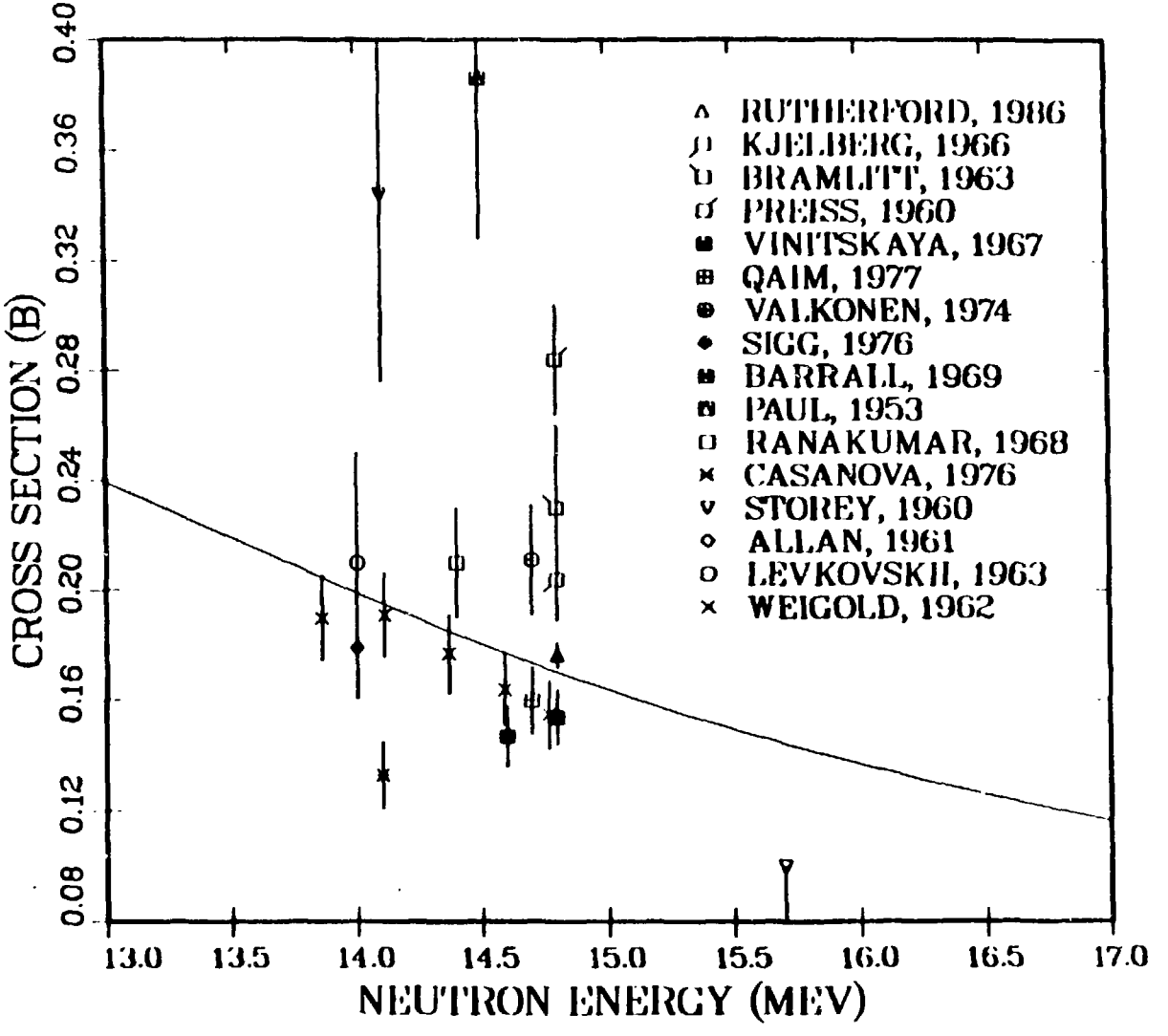

Figure 5.5 Comparison of Theoretical and Experimental Values Obtained for ^{64}Zn (n, p) ^{64}Cu Cross Sections from 13.0 – 17.0 MeV

Figure 5.4 and 5.5. For example, the results presented by Nemilov in 1978 are low compared with Santry's data, and both fall lower than the calculations [35,36]. The experimental data presented by Smith agree well with the theoretical calculations up to 3.0 MeV and then diverge rapidly up to 10.0 MeV [37].

In Figure 5.5 the results presented by Santry in 1972 show good agreement [36]. Additionally, Santry shows good overall agreement with both the (n,2n) and the (n,p) measurements and with the corresponding theoretical values calculated in this work at a wide range of energies.

5.5 **Conclusions**

The present experiment has resulted in values for the ^{64}Zn $(n,2n)^{63}Zn$ and ^{64}Zn $(n,p)^{63}Cu$ cross sections that are more accurate than those obtained previously. As seen in Table 5.4 the results presented here agree well with the previously measured values of the (n,2n) reaction. Similarly, the (n,p) measurements are well within previously measured values as shown in Table 5.5. The reduced uncertainty of these measurements gives additional confidence in them. The use of complementary theoretical calculations has extended the applicability of these values to other neutron energies.

To conclude, then, it has been shown in the spirit of philosophical deduction and scientific research that these specific cross sections have been remeasured accurately with theoretical predictions coinciding very accurately as well. In the spirit in which the text was written, Lucretius said, "Now do you see that, as we said a little earlier, in

the case of the same atoms it often makes a great difference with what other atoms they are in contact, in what arrangements they are held, and in what ways they set others in motion and are moved themselves; and do you not see that the same atoms with slight changes among themselves create flames and beams?" [3].

Table 5.4

Other Values of the ^{64}Zn (n,2n)^{63}Zn Cross Section

Author	E_n(MeV)	Cross Section (mb)	Reference
Weigold	14.6	165.0 ± 13	[33]
Csikai	14.6	200.0 ± 13	[38]
Cohen	14.6	270.0 ± 25	[39]
Sigg	14.6	146.0 ± 11	[40]
Paulsen	14.6	196.0 ± 14	[31]
Csikai	14.7	225.0 ± 25	[38]
Valkonen	14.7	190.0 ± 20	[41]
Weigold	14.7	182.0 ± 15	[33]
Mitra	14.8	102.0 ± 10	[42]
Preiss	14.8	254.0 ± 20	[43]
Bramlett	14.8	153.0 ± 36	[44]
Chatterjee	14.8	165.0 ± 16	[45]
Rutherford	14.8	199 ± 6	
Cohen	14.9	300.0 ± 20	[39]
Paulsen	15.0	227.0 ± 16	[31]

Table 5.5

Other Values Obtained for the ^{64}Zn (n,p)^{64}Cu Cross Section

Author	E_n(MeV)	Cross Section (mb)	Reference
Weigold	14.6	164.0 ± 13	[33]
Barrall	14.6	147.0 ± 10	[46]
Sigg	14.6	147.0 ± 11	[40]
Santry	14.7	166.0 ± 10	[36]
Valkonen	14.7	211.0 ± 20	[41]
Qaim	14.7	160.0 ± 12	[47]
Gabbard	14.7	185.0 ± 20	[48]
Santry	14.8	166.0 ± 10	[36]
Vinitskaya	14.8	154.0 ± 10	[49]
Preiss	14.8	284.0 ± 20	[43]
Bramlett	14.8	230.0 ± 30	[44]
Kjelberg	14.8	204.0 ± 15	[50]
Rutherford	14.8	176.5 ± 4	
Gabbard	15.0	197.0 ± 20	[48]

6.0 Future Work

Recommendations for future work include extending the data base of precise values to other neutron energies. This would further complement the theoretical work and provide additional accuracy for the applied data users. Also, theoretical calculations should be performed for the ^{66}Zn and ^{68}Zn isotopes because they along with ^{64}Zn are the components of natural zinc. The experimental data base should also be extended for these two isotopes as well as for ^{64}Zn.

Since the most recent work on the decay scheme of ^{63}Zn was performed in 1947, it needs to be remeasured and/or reevaluated to reduce the error associated with its decay. The half-life determination should also be reevaluated.

Currently there is no existing data for zinc or for zinc isotopes in the ENDF/B-V library; therefore the results of the present theoretical/experimental analysis will be incorporated into the library.

REFERENCES

[1] "Report to the DOE Nuclear Data Committee", Brookhaven National Laboratory, May 1985.

[2] E. T. Cheng, D. R. Mathews, and R. K. Shultz, "Coordination of Magnetic Fusion Energy Nuclear Data Needs", Annual Report for FY 1983, GA-A16886, GA Technologies.

[3] Lucretius, On Nature, Book One, II, 240-250. The Library of Liberal Arts, c-1965.

[4] F. Ghanberri, Ph.D dissertation, UNM, (1986).

[5] D. I. Garber, and R. R. Kinsey, Neutron Cross Sections, Volume II, January, 1976.

[6] E. D. Arthur and P. G. Young, GNASH, LANL, LA-6947 (1977).

[7] F. Ghanbari and J. C. Robertson, "The Cu-63(n,2n)Cu-62 and Cu-65(n,2n)Cu-64 Cross Sections at 14.8 MeV", Proceedings Int. Nucl. Data Conf. (1985).

[8] E. D. Arthur and P. G. Young, "Evaluated Neutron Cross Sections for Fe-54,56 to 40 MeV", LANL, LA-8626-MS (1980).

[9] P. Kruger, Principles of Activation Analysis, (John Wiley & Sons, Inc., New York 1971).

[10] G. F. Knoll, Radiation Detection and Measurement, (John Wiley & Sons, Inc., New York, 1979).

[11] S. S. Nargolwalla and E. P. Przybylowicz, Activation Analysis with Neutron Generators, (John Wiley & Sons, Inc., New York, 1973).

[12] M. Rowland and J. C. Robertson, Proc. ANS Winter Meeting (1984).

[13] P. Christmas, S. M. Judge, T. B. Ryves, and D. Smith, Nuc. Inst. and Methods, 215, 397-408, (1983).

[14] M. Uhl, "Recent Advances in Nuclear Model Code Developments", Nuclear Theory for Applications, IAEA Conf., Trieste (1982).

[15] O. Bersillon, computer program SCATOP, (Centre D'Etudes de Bruyers-le-Chatel, France).

[16] C. M. Lederer and V. S. Shirley, Table of the Isotopes, (John Wiley & Sons, Inc., New York, 1978).

[17] A. Gilbert and G. W. Cameron, Can. Jour. Phys. 43, 1446, (1965).

[18] P. D. Kunz, "DWUCK-A Distorted Wave Born Approximation Program", unpublished.

[19] National Nuclear Data Library, Brookhaven National Laboratory, N.Y.

[20] W. Hauser and H. Feshbach, Phys. Rev. 87, 366, (1952).

[21] J. M. Blatt and U. F. Weisskopf, Theoretical Nuclear Physics (John Wiley & Sons, Inc., New York, 1952).

[22] C. Kalbach-Cline, "Residual Two Body Matrix Elements for Preequilibrium Calculations", Nucl. Phys. A-210, 590, (1973).

[23] R. R. Johnson and G. D. Jones, "The Zn-64(p,p')Zn-64 and Zn-64(p,d)Zn-63 Reactions at 26 MeV", Nucl. Phys. A-122, 657, (1968).

[24] S. Kaplan, Nuclear Phys., (Addison - Wesley Publishing Company, 1964).

[25] O. Bersillon, "SCAT2 - A Spherical Optical Model Code," in "Progress Report of the Nuclear Physics Division, Bruyeres-le-Chatel 1977," CEA-N-2037, 111 (1978).

[26] E. D. Arthur, personnel communication.

[27] M. Mughabghab, Neutron Cross Sections, (Vol. 1, Academic Press, 1981).

[28] C. Harper, "Experimental and Theoretical Neutron Cross Sections at 14 MeV", Ph.D dissertation, Auburn U. (1974).

[29] D. G. Foster Jr., D. W. Glasgow, "Neutron Total Cross Sections 2.5-15 MeV.", Phys. Rev. C3, 604 (1971).

[30] P. Axel, "Electric Dipole Ground State Transition Width Strength Functions", Phys. Rev. 126, 671 (1962).

[31] A. Paulsen and H. Liskien, Nukleonik, 7, 117 (1965).

[32] M. Bormann and B. Lammers, "Excitation Functions of (n,p) and (n,2n) Reactions for Some Isotopes of K, Mn, Zn, Cu," Nucl. Phys., A-130, 195-208 (1969).

[33] E. Weigold, R. N. Glover, "Some Activation Measurements and a Comparison with Theoretical (n,2n) Cross Sections and Isomeric Cross Section Ratios", Nucl. Phys., 32, 106 (1962).

[34] M. N. Rao, Nucl. Data, B3-3, 4-43 (1970).

[35] A. Nemilov, Nucl. Data, B3-3, 4-43 (1978).

[36] D. C. Santry and J. P Butler, "Excitation Curves for the Reactions of Fast Neutrons with Zinc", Can. J. Phys., 50, 2536 (1972).

[37] D. L. Smith and J. W. Meadows, "Cross Sections for (n,p) Reactions on Al-27, Ti-46,47,48, Fe-54,56, Ni-58, Co-59 and Zn-64", ANL/NDM-10, Argonne National Laboratory (1975).

[38] J. Csikai and G. Peto, "Influence of Direct Scattering on (n,2n) Cross Sections", AHP, 23, 87 (1967).

[39] A. V. Cohen and P. H. White, "The Excitation Curves of Some (n,p) Processes Induced by Neutrons of 12.5-17.5 MeV Energy," Nucl.Phys., 1, 72-84 (1956).

[40] T. Sigg, " Fast Neutron Induced Reaction Cross Sections and their Systematics", T. Sigg, 1976.

[41] M. Valkonen, "Studies of 14 MeV Neutron Activation Cross Sections with Special Refernece to the Capture Reaction", JIN, 36, 715 (1974).

[42] B. Mitra, "The (n,2n) Reaction Cross Section of P-31, Zn-64, Ga-69 and Ag-107 For 14.8 MeV Neutrons", Int. J. Phys., 41, 752 (1967).

[43] I. L. Preiss and R. W. Fink, "New Isotopes of Cobalt, Activation Cross Sections of Nickel, Cobalt and Zinc for 14.8 MeV Neutrons", Nucl. Phys., 15, 326 (1960).

[44] E. T. Bramlett and R. W. Fink, "Rare Nuclear Reactions Induced by 14.8 MeV Neutrons", Phys. Rev., 131, 2649 (1963).

[45] A. Chaterjee, A. Nath, A. M. Ghose, "Measurement of (n,2n) Cross Sections for Fast Neutrons", Kanpur, 363, (1967).

[46] R. C. Barrall, J. A. Holmes, M. Silbergeld, "High Energy Neutron Cross Section Validation and Neutron Flux Spectrum Using the Henre Source", R, AFWL-TR-68-134 (1969).

[47] S. M. Qaim, "Activation Cross Sections, Isomeric Cross-Section Ratios and Systematics of (n,2n) Reactions at 14-15 MeV", Nucl. Phys., A185, 614-624 (1972).

[48] F. Gabbard and B. D. Kern, "Cross Sections for Charged Particle Reactions Induced in Medium Weight Nuclei by Neutrons in the Energy Range 12-18 MeV", Phys. Rev., 128, 1276-1281 (1962).

[49] G. P. Vinitskaya, V. Levkovshij, V. V. Sokol'skij, I. V. Kazachevkij, "Cross Sections of the (n,p) and (n.alpha) Reactions At Neutron Energy 14.8 MeV", SCISRS Listing Brookhaven National Laboratory.

[50] A. Kjelberg, A. C. Pappas, E. Steinnes, "Cross Sections of Some (n,p) and (n,alpha) Reactions Induced By 14.8 MeV Neutrons", RCA, 5, 28 (1966).